Institutionen för systemteknik
Department of Electrical Engineering

Examensarbete

State Estimation of UAV using Extended Kalman Filter

Examensarbete utfört i Reglerteknik
vid Tekniska högskolan vid Linköpings universitet
av

Thom Magnusson

LiTH-ISY-EX--13/4662--SE

Linköping 2013

Linköpings universitet
TEKNISKA HÖGSKOLAN

Department of Electrical Engineering
Linköpings universitet
SE-581 83 Linköping, Sweden

Linköpings tekniska högskola
Linköpings universitet
581 83 Linköping

State Estimation of UAV using Extended Kalman Filter

Examensarbete utfört i Reglerteknik
vid Tekniska högskolan i Linköping
av

Thom Magnusson

LiTH-ISY-EX--13/4662--SE

Handledare: **Manon Kok**
ISY, Linköpings universitet
Magnus Degerfalk
Instrument Control Sweden

Examinator: **Fredrik Gustafsson**
ISY, Linköpings universitet

Linköping, 21 May, 2013

Avdelning, Institution
Division, Department

Division of Automatic Control
Department of Electrical Engineering
Linköpings universitet
SE-581 83 Linköping, Sweden

Datum
Date

2013-05-21

Språk
Language

☐ Svenska/Swedish
☒ Engelska/English
☐ _____

Rapporttyp
Report category

☐ Licentiatavhandling
☒ Examensarbete
☐ C-uppsats
☐ D-uppsats
☐ Övrig rapport
☐ _____

ISBN
__

ISRN
LiTH-ISY-EX--13/4662--SE

Serietitel och serienummer **ISSN**
Title of series, numbering __

URL för elektronisk version
http://www.control.isy.liu.se
http://www.ep.liu.se

Titel
Title State Estimation of UAV using Extended Kalman Filter

Författare Thom Magnusson
Author

Sammanfattning
Abstract

In unmanned systems an autopilot controls the outputs of the vehicle without human interference. All decisions made by the autopilot will depend on estimates delivered by an *Inertial Navigation System*, INS. For the autopilot to take correct decisions it must rely on correct estimates of its orientation, position and velocity. Hence, higher performance of the autopilot can be achieved by improving its INS. Instrument Control Sweden AB has an autopilot developed for fixed wing aircraft. The focus of this thesis has been on investigating the potential benefits of using Extended Kalman filters for estimating information required by the control system in the autopilot. The Extended Kalman filter is used to fuse sensor measurements from accelerometers, magnetometers, gyroscopes, GPS and pitot tubes. The filter will be compared to the current *Attitude and Heading Reference System*, AHRS, to see if better results can be achieved by utilizing sensor fusion.

Nyckelord
Keywords key1, key2

Abstract

In unmanned systems an autopilot controls the outputs of the vehicle without human interference. All decisions made by the autopilot will depend on estimates delivered by an *Inertial Navigation System*, INS. For the autopilot to take correct decisions it must rely on correct estimates of its orientation, position and velocity. Hence, higher performance of the autopilot can be achieved by improving its INS. Instrument Control Sweden AB has an autopilot developed for fixed wing aircraft. The focus of this thesis has been on investigating the potential benefits of using Extended Kalman filters for estimating information required by the control system in the autopilot. The Extended Kalman filter is used to fuse sensor measurements from accelerometers, magnetometers, gyroscopes, GPS and pitot tubes. The filter will be compared to the current *Attitude and Heading Reference System*, AHRS, to see if better results can be achieved by utilizing sensor fusion.

Acknowledgments

I would like to send my appreciation to everyone at Instrument Control Sweden AB for providing me with the opportunity to do this master thesis. Thanks to Magnus Degerfalk, supervisor at Instrument Control Sweden AB, for all support and guidance. I would also like to thank Manon Kok, supervisor at Linköping University, for always having time for questions and for providing me with new ideas. I have also had great support from my examiner, Fredrik Gustafsson, Linköping University, and would like to thank him as well for helping me during this thesis.

Contents

Chapter 1

Introduction

1.1 Background

Unmanned Aerial Vehicles, UAV, have been developed since the first world war. At this time they were used as target drones to train anti-air crews and they were controlled remotely from the ground. The development of the conventional UAV, as we know it today, was set in motion by *United States Air Force*, USAF, in 1959 to avoid casualties during air surveillance. Since then there has been an immense effort to improve their capabilities. At this time, the components needed to build a UAV were extremely expensive and navigation precision was poor. In absence of a Global Navigation Satellite System, GNSS, the UAV had to rely on an *Inertial Navigation System*, INS, for long range flights. This generated a great effort in developing an INS, which is using accelerometers and gyroscopes to determine attitude, velocities and position. Consequently the first generations of surveillance UAVs did not succeed in taking photos at the correct locations. One of the first navigational improvements was achieved when implementing a Doppler navigation radar to the UAVs. This type of UAV was flown in 1968.

When the American GNSS, *Global Positioning System*, GPS, was developed and live feeds from on-board cameras could be transmitted to the ground, the modern UAV as we know it today was developed. At the same time, technological improvements allowed for higher precision UAVs and the price on vital components such as high precision gyroscopes and accelerometers started to drop. This new possibility of developing cheaper and more effective UAVs has created interest in the civil market. Today, UAVs are being used in a variety of areas from livestock monitoring to hurricane research.

These new markets have generated a need for cheap and easy to use UAVs. With the arrival of smaller and cheaper sensors the competition of creating cheap, small and reliable UAVs has grown. Therefore it is now important to develop reliable control and navigation systems with commercially available sensors.

Figure 1.1. The ground control station developed by Instrument Control Sweden.

1.2 Motivation

Instrument Control Sweden develops and sells complete solutions for UAV operation with ground control stations, autopilot and high end software. The Unmanned Aircraft System, SkyView, allows the user to control and manage several UAVs. The ground control station can be seen in Figure 1.1 and the SkyView user interface in Figure 1.2. The autopilot developed by Instrument Control Sweden is called EasyPilot and can be seen in Figure 1.3.

It is from SkyView the user decides what the UAV is going to do. From here the UAV can be controlled in a stabilized mode and mission mode. In stabilized mode the user controls the UAV directly from the ground station. In this case, EasyPilot controls the aircraft while the user indicates what he wants the aircraft to do. In mission mode a flight path is uploaded to EasyPilot. EasyPilot then controls the aircraft to follow the uploaded flight path.

To be able to control the aircraft efficiently, information about attitude, heading, position and velocities are required. If incorrect attitude estimations are acquired the performance of the control loops are irrelevant. All this information is delivered by EasyPilot's sensor unit. The main goal of this master thesis is to improve this sensor unit and to enable the control system to work more efficiently.

The main idea is to use an Extended Kalman Filter, EKF, for state estimation. An EKF is a powerful way to utilize and merge information from several different sensors, and still take system dynamics into account. When developing an Extended Kalman filter state dynamics must be derived. Then a mathematical relation between sensor measurements and state dynamics are defined. The state dynamics then propagates with time and at every measurement the state dynamics are updated to minimize the deviation from the true states.

Figure 1.2. A screenshot from the ground control station system Sky View. Here, a live 3D feed of the vehicle can be seen to the upper left, the attitude estimation to the upper right and the planned mission down to the left.

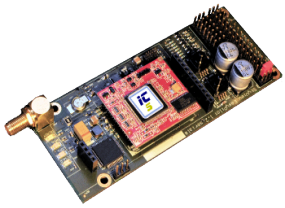

Figure 1.3. The autopilot, EasyPilot, developed by Instrument Control Sweden.

1.3 Hardware

The EasyPilot has two main processors, one for the main control system and one for the sensor unit. All the available sensors are connected to the sensor units main processor. The sensor unit communicates with the control unit and the sensors, and the control unit communicates with the ground control station and the servos of the aircraft.

The following sensors are mounted on the platform and will be utilized in the Extended Kalman filter:

- 3 axis gyroscope
- 3 axis accelerometer
- 3 axis magnetometer

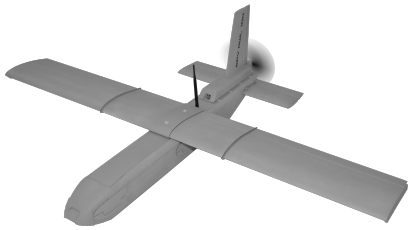

Figure 1.4. The Spy Owl 100 is a UAV designed for training purposes. It is a rigid construction on which the EasyPilot has been developed and evaluated.

- GPS
- Static and dynamic pressure sensors

The current processor mounted on the chip is a fixed point processor at approximately 70MHz. The evaluation of the Extended Kalman filter will be based on real data from flights using an in-house developed UAV called Spy Owl 100, see Figure 1.4.

Chapter 2

Coordinate systems

In aviation, different coordinate systems are used depending on what information is to be described. When navigating around the earth, the position must be described in a comprehensive and convenient way. If the locations of the earth are described in a way that allows us to describe positions all over the world, low velocities would be hard to describe relative to this frame. Therefore another coordinate system must be used when handling low velocities.

The orientation of a vessel is always relative to another coordinate system. When an aircraft is accelerating straight forward seen from inside the plane, it can be oriented in way so that it is accelerating north-east and climbing relative to the earth. Therefore, there must also be a coordinate system fixed to the aircraft because it is here all the sensors are mounted.

All the information that is easily described within a coordinate system, will be described within this coordinate system, thus simplifying calculations. Then the information can be transformed between different coordinate systems. An example of this is how we describe position using longitude and latitude. This is an easy way of describing a position on the earth, but it is rather unusual to describe velocities as longitudes per second. Another example is when the aircraft is accelerating straight forward, seen from within the aircraft. This information is not interesting, unless we know in which direction relative to the earth it is accelerating.

This chapter describes different coordinate systems that are important in avionics and how to transform them into other coordinate systems.

2.1 Earth-Centered, Earth-Fixed

Earth-Centered, Earth-Fixed, ECEF, is a Cartesian coordinate system, (X^E, Y^E, Z^E) (superscript E for earth), with its origin in the earth's center of mass and with fixed axes with respect to the earth as seen in Figure 2.1. This means that the coordinate system rotates with the earth. The Z^E-axis is aligned with the north pole of the earth and the X^E-axis is aligned with the Greenwich Prime. The Y^E-axis is defined so that a right handed system is achieved. The (X^E, Y^E)-plane

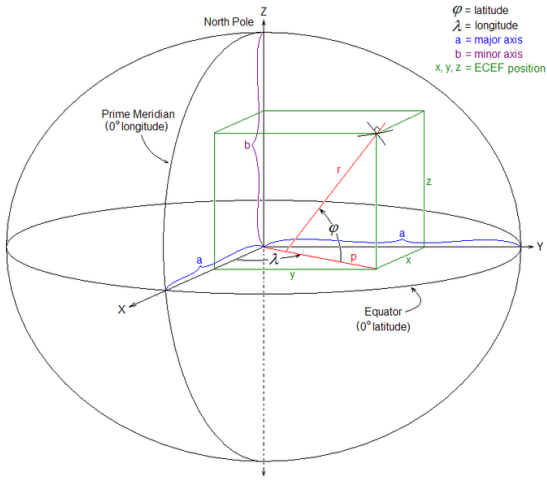

Figure 2.1. The Earth Centered Earth Fixed coordinate system, green, relative to conventional longitude and latitude degrees, black.

then defines the equatorial plane.

A position on the earth is often decided using a world geodetic system, presenting the data in longitude, latitude and height over sea level. Longitude, (λ), is the angle between the Greenwich meridian and the position. Latitude, (ϕ), is the angle between the equatorial plane and the position. The height is defined as the height over a reference surface, such as WGS84 which is explained in more detail in the next section.

World geodetic system

A world geodetic system, WGS, is a reference that defines a relationship between the Cartesian coordinate system and longitude-latitude. The earth is modelled as a rotationally symmetric ellipsoid with the system's origin in the earth's center of mass and the IERS, *International Earth Rotation and Reference Systems Service*, reference meridian as zero longitude. In Table 2.1, the parameters defining the reference surface for WGS84 are presented. The flattening is the relationship between the ellipsoid radii, a and b according to

$$b = a(1 - f). \tag{2.1}$$

Here, the flattening, f, is a measurement of how much the ellipsoid deviates from a sphere.

The conversion from longitude-latitude with height over sea level to ECEF

Description	Parameter	Value
Major radius	a	6378137 [m]
Minor radius	b	6356752.3142 [m]
Flattening	f	1/298.257223563
First eccentricity	e_1	$\sqrt{1-\frac{b^2}{a^2}}$
Second eccentricity	e_2	$\sqrt{\frac{a^2}{b^2}-1}$
IERS reference meridian	-	102.5[m] east of the Greenwich Prime.

Table 2.1. Parameters defining the reference for WGS84.

Cartesian coordinates is given by:

$$X = (N+h)\cos(\phi)\cos(\lambda) \tag{2.2}$$
$$Y = (N+h)\cos(\phi)\cos(\lambda) \tag{2.3}$$
$$Z = (\frac{b^2}{a^2}N+h)\sin(\phi) \tag{2.4}$$

where

$$N = \frac{a}{\sqrt{1-e_1^2\sin^2(\phi)}} \tag{2.5}$$

The conversion from ECEF Cartesian coordinates to longitude-latitude with height over sea level is given by:

$$\lambda = \arctan(\frac{X}{Y}) \tag{2.6}$$
$$\phi = \arctan\left(\frac{Z+e_2 b\sin^3(\theta)}{p-e_1^2 a\cos^3(\theta)}\right) \tag{2.7}$$
$$h = \frac{p}{\cos(\phi)} - N \tag{2.8}$$

where

$$p = \sqrt{X^2+Y^2} \tag{2.9}$$
$$\theta = \arctan(\frac{Za}{pb}) \tag{2.10}$$

The Global Positioning System uses the WGS84, which is the latest revision of the world geodetic system. This revision is accurate to up to a meter and is maintained by the *International Earth Rotation and Reference System Service (IERS)*.

2.2 Local Geodetic Frame

A local geodetic frame is a coordinate system that is local in a point somewhere over the earth's surface. This is often used as a navigation frame for aerial vessels

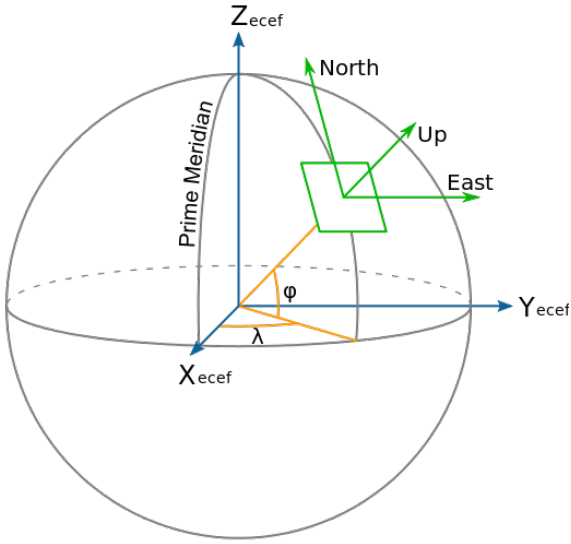

Figure 2.2. The ENU-frame relative to ECEF coordinate system.

and is fixed in the vessels center of mass. Two axes make up a tangential plane to the surface of the earth and the third axis is orthogonal to this plane. There are two commonly used local frames:

ENU - East,North,Up

NED - North,East,Down

These are both right-handed and the choice of frame depends on the application. The north component in this frame points to the geographical north pole, which is defined by the earth's rotational axis, rather than the magnetic north pole which is defined by the magnetic field generated by the earth's core. These two differs from each other and the magnetic north pole is not constant with time. The down/up component is aligned with the earth's gravity field and the east component is defined as east relative to the geographical north pole.

In aviation it is preferred to use a NED-frame due to the fact that positive numbers are defined down. The ENU-frame can be seen in Figure 2.2 and the NED frame is equivalently constructed.

2.2.1 Velocity relations to WGS

If different coordinate systems are to be used for position, WGS, and velocity, NED, the propagation of the position with respect to NED velocities must be

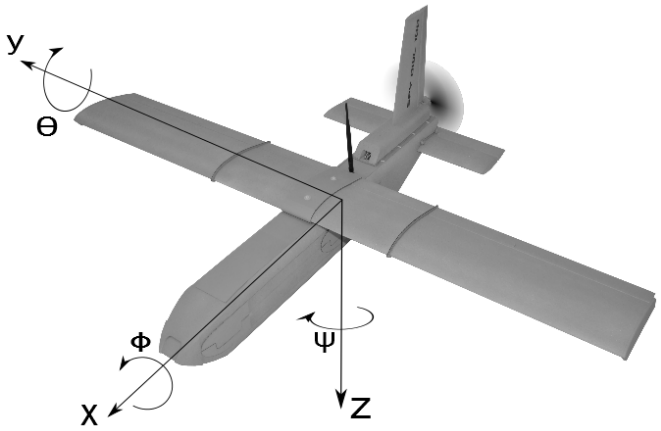

Figure 2.3. The body fixed coordinate system with the rotations defined as ϕ around the x-axis, θ around the y-axis and ψ around the z-axis.

utilized in the state dynamics. These relationships are given by

$$\dot{\lambda} = \frac{V_E}{(R_p + h)\cos\phi} \tag{2.11}$$

$$\dot{\phi} = \frac{V_N}{R_m + h} \tag{2.12}$$

where R_p and R_m are given by

$$R_p = \frac{a}{(1 - \epsilon_1^2 \sin^2\phi)^{1/2}} \approx a \tag{2.13}$$

$$R_m = \frac{a(1 - \epsilon_1^2)}{(1 - \epsilon_1^2 \sin^2\phi)^{3/2}} \approx a. \tag{2.14}$$

2.3 Body frame

The body frame is fixed to the aircraft's center of mass where the axes are defined as follow:

x - Straight forward through the nose of the plane.

y - Right of the plane.

z - Down of the plane.

In avionics rotations around these axes are called yaw, pitch and roll. An overview of the body frame can be seen in Figure 2.3. The angles themselves define the aircraft's orientation with respect to a local geodetic frame whilst the rotation rates define the aircraft's motion.

2.4 Rotation between frames

In a navigation systems, GPS, magnetometers, accelerometers, gyroscopes and pitot tubes are standard sensors. The goal is to estimate position, attitude and heading but the measurements and estimates are in different coordinate systems. To be able to fuse the measurements in a proper manner there must be a mathematical connection between measurements and states to be estimated in different frames. Therefore, some measurements or states must be rotated into another frame. Mainly, there are rotations between the body frame and the NED-frame.

There are three common methods to accomplish these rotations:

Euler angles - When using Euler angles to rotate between frames, three separate rotations around single axes are performed. This is an intuitive way of rotating between frames but is singular when pitch is 90 degrees.

Direction cosine matrix - When using Direction cosine matrix the rotation from one frame into another is performed with a single matrix multiplication. This method has no singularities but nine values to keep track of.

Quaternions - When using quaternions to rotate between frames, a single rotation is performed around an imaginary vector. This method has no singularities and only four states which is fewer than Direction cosine matrix. The main disadvantage is that there is no intuitive way of interpreting the quaternions.

2.4.1 Euler angles

The Euler angles are coupled to the notations used in the description of the body frame and the NED-frame. These angles themselves represents the attitude of the plane. The Euler angles will be explained using the following notations.

Yaw, (ψ) - The yaw angle is the rotation around the body frame's z-axis. The angular difference between the body's x-axis and the N-axis in the NED frame is called heading.

Pitch, (θ) - The pitch angle is the angle between the body's x-axis and the plane represented by N and E axes in the NED frame.

Roll, (ϕ) - The roll angle is the rotation around the body's x-axis. If the plane is flying straight forward but upside down, the roll angle is 180 degrees.

An illustration of the Euler angles can be seen in Figure 2.4.

Euler angles are used to describe how a body is oriented with respect to another frame. When rotating a right handed coordinate system using Euler angles, three successive rotations are done, one on each axis. This can be achieved by:

- Rotate ψ degrees around the body's z-axis.
- Rotate θ degrees around the body's y-axis.

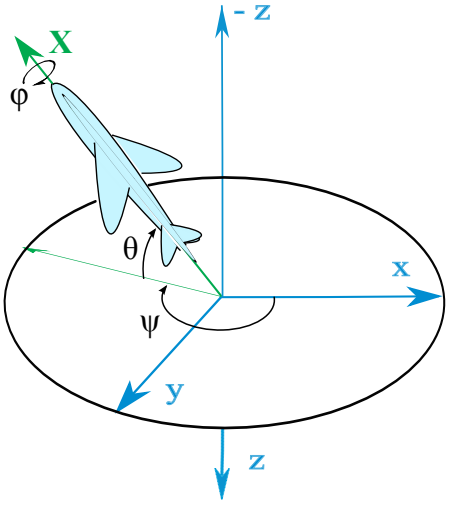

Figure 2.4. The Euler angles for a rotation between a body frame and the NED frame.

- Rotate ϕ degrees around the body's x-axis.

These rotations can be represented as three different rotation matrices [21, 17] as stated in equations (2.15-2.17)

$$C_\psi = \begin{bmatrix} \cos\psi & \sin\psi & 0 \\ -\sin\psi & \cos\psi & 0 \\ 0 & 0 & 1 \end{bmatrix} \tag{2.15}$$

$$C_\theta = \begin{bmatrix} \cos\theta & 0 & -\sin\theta \\ 0 & 1 & 0 \\ \sin\theta & 0 & \cos\theta \end{bmatrix} \tag{2.16}$$

$$C_\phi = \begin{bmatrix} 1 & 0 & 0 \\ 0 & \cos\phi & \sin\phi \\ 0 & -\sin\phi & \cos\phi \end{bmatrix} \tag{2.17}$$

These separate rotations can be put together into one rotation matrix. A rotation from the NED frame into the body frame can then be described as

$$C_n^b = C_\psi C_\theta C_\phi \tag{2.18}$$

where the notation with subscript n and superscript b means from NED-frame to body-frame. If (2.18) is calculated using equations (2.15)-(2.17) we get a rotation

matrix according to:

$$C_n^b = \begin{bmatrix} \cos\theta\cos\psi & \cos\theta\sin\psi & -\sin\theta \\ \sin\phi\sin\theta\cos\psi \\ -\cos\phi\sin\psi & \sin\phi\sin\theta\sin\psi \\ +\cos\phi\cos\psi & \sin\phi\cos\theta \\ \cos\phi\sin\theta\cos\psi \\ +\sin\phi\sin\psi & \cos\phi\sin\theta\sin\psi \\ -\sin\phi\sin\psi & \cos\phi\cos\theta \end{bmatrix}. \tag{2.19}$$

The fact that,

$$\begin{aligned} \det(C_\psi) = \det(C_\theta) = \det(C_\phi) = 1 \\ C_\psi = C_\psi^T \\ C_\theta = C_\theta^T \\ C_\phi = C_\phi^T \end{aligned}$$

implicates that the rotation matrix is orthonormal as well. The rotation from the body frame into the NED frame is then given by

$$C_b^n = (C_n^b)^{-1} = (C_n^b)^T. \tag{2.20}$$

since C_b^n is an orthonormal rotation matrix.

Propagation of Euler angles

The Euler angles are continuously updated through integration of the body's rotation rates, ω_x, ω_y and ω_z. The relationship between body rates and Euler angles propagation are derived in [21] and is given by

$$\begin{bmatrix} \omega_x \\ \omega_y \\ \omega_z \end{bmatrix} = \begin{bmatrix} \dot{\phi} \\ 0 \\ 0 \end{bmatrix} + C_\phi \begin{bmatrix} 0 \\ \dot{\theta} \\ 0 \end{bmatrix} + C_\phi C_\theta \begin{bmatrix} 0 \\ 0 \\ \dot{\psi} \end{bmatrix}. \tag{2.21}$$

Solving (2.21) for $\dot{\psi}$, $\dot{\theta}$ and $\dot{\phi}$ gives the equations

$$\dot{\phi} = (\omega_y \sin\phi + \omega_z \cos\phi)\tan\theta + \omega_x \tag{2.22}$$

$$\dot{\theta} = \omega_y \cos\theta - \omega_z \sin\phi \tag{2.23}$$

$$\dot{\psi} = (\omega_y \sin\phi + \omega_z \cos\phi)\frac{1}{\cos\theta}. \tag{2.24}$$

As seen in (2.24) there is a possibility of division by zero, which results in the singularity mentioned before. In most ground applications and most helicopter applications this is not an issue. If a car or equivalent has a pitch of 90°, singularity in the Euler angle propagation is probably not the biggest problem. But this can be used in avionics as well, helicopters for example do not usually fly with 90° pitch.

2.4.2 Direction cosine matrix

When using Direction cosine matrix, the rotation is performed by a single matrix multiplication. It also has no singularities which makes it useful in more applications. Transforming an arbitrary vector from a coordinate system (i) to a coordinate system (j) is done by multiplying the vector to be rotated with a matrix [21, 17],

$$\nu_j = C_i^j \nu_i \tag{2.25}$$

where

$$C_i^j = \begin{bmatrix} c_{11} & c_{12} & c_{13} \\ c_{21} & c_{22} & c_{23} \\ c_{31} & c_{32} & c_{33} \end{bmatrix}. \tag{2.26}$$

Each row and column in the Direction cosine matrix must be orthogonal and unit. This gives that there are three degrees of freedom.

The method itself is straightforward, but unlike the Euler angles the individual elements do not represent the body's attitude in an intuitive way. Therefore a conversion to Euler angles is often done so that the attitude of a body relative to a frame can be interpreted.

Propagation of Direction cosine matrices

We approximate the derivative of the Direction cosine matrix with

$$\dot{C_i^j} = \lim_{\delta t \to 0} \frac{C_i^j(t + \delta t) - C_i^j(t)}{\delta t}. \tag{2.27}$$

At the time, $t + \delta t$, the rotation matrix differs from time t. The difference can be seen as a rotation between two frames, giving

$$C_i^j(t + \delta t) = A(t) C_i^j(t) \tag{2.28}$$

where A is a rotation matrix defined as

$$A(t) = [I_{3x3} + \delta\Psi], \tag{2.29}$$

$$\tag{2.30}$$

where

$$\Psi = \begin{pmatrix} 0 & -\psi & \theta \\ \psi & 0 & -\phi \\ -\theta & \phi & 0 \end{pmatrix}. \tag{2.31}$$

We can then rewrite (2.27) to

$$\dot{C_i^j} = \lim_{\delta t \to 0} \frac{\delta\Psi}{\delta t}. \tag{2.32}$$

The derivatives of the angles yields the rotation rate of the body and we get

$$\dot{C_i^j} = C_i^j \Omega \tag{2.33}$$

where

$$\Omega = \begin{pmatrix} 0 & -\omega_z & \omega_y \\ \omega_z & 0 & -\omega_x \\ -\omega_y & \omega_x & 0 \end{pmatrix}. \tag{2.34}$$

The Direction cosine matrix has an advantage over Euler angles due to the fact that it lacks singularities. There are only three degrees of freedom, but there are nine elements to update in every iteration. If a rotation is to be embedded in an Extended Kalman filter this is a big drawback since it is desirable to have as few states as possible to reduce complexity.

Relations to Euler angles

When using Euler angles the three consecutive rotations were multiplied together to form a single rotation matrix. Since Direction cosine matrix is a rotation performed by a single matrix multiplication, this matrix must be equal to the rotation matrix achieved by using Euler angles according to

$$C^j_{i,\text{Euler}} = C^j_{i,\text{DCM}}. \tag{2.35}$$

From the Direction cosine matrix we can derive the Euler angles from the relationship

$$\begin{bmatrix} \cos\theta cos\psi & \cos\theta\sin\psi & -\sin\theta \\ \sin\phi\sin\theta\cos\psi & \sin\phi\sin\theta\sin\psi & \sin\phi\cos\theta \\ -\cos\phi\sin\psi & +\cos\phi\cos\psi & \\ \cos\phi\sin\theta\cos\psi & \cos\phi\sin\theta\sin\psi & \cos\phi\cos\theta \\ +\sin\phi\sin\psi & -\sin\phi\sin\psi & \end{bmatrix} = \begin{bmatrix} c_{11} & c_{12} & c_{13} \\ c_{21} & c_{22} & c_{23} \\ c_{31} & c_{32} & c_{33} \end{bmatrix} \tag{2.36}$$

by comparing the elements and get

$$\phi = \arctan\left(\frac{c_{32}}{c_{33}}\right) \tag{2.37}$$

$$\theta = \arcsin\left(-c_{31}\right) \tag{2.38}$$

$$\psi = \arctan\left(\frac{c_{21}}{c_{11}}\right). \tag{2.39}$$

There exists a singularity at 90° pitch here as well when converting from Direction cosine matrix to Euler angles. In these cases other types of conversions to Euler angles must be used.

2.4.3 Quaternions

The theory of quaternions was described by Sir William Rowan in 1843. The usage of quaternions as a rotation between frames was described by Benjamin Olinde Rodrigues. So the rotation method described in this section is often called Euler-Rodrigues' rotation formula. In avionics combined with Kalman filtering,

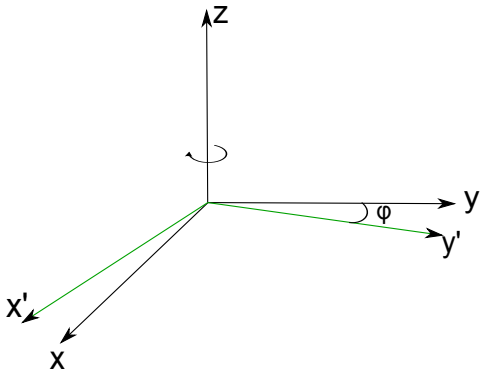

Figure 2.5. Rotation from x, y to $x\prime, y\prime$ is done by rotating ϕ degrees around z.

this is probably the most common method to rotate between frames. There are no singularities and four states to update, which is fewer than the Direction cosine matrix.

The idea of using quaternions is that we can rotate a three dimensional frame into another around a vector that is orthogonal to the three dimensional space. This can be exemplified by the rotation of a two dimensional plane. The relationship between the two frames, (x, y) and $(x\prime, y\prime)$, in Figure 2.5 is a rotation of ϕ degrees around the z-axis.

A 4-dimensional quaternion is defined as

$$\mathbf{q} = q_0 + q_1\mathbf{i} + q_2\mathbf{j} + q_3\mathbf{k} = \begin{bmatrix} q_0 & q_1 & q_2 & q_3 \end{bmatrix} \begin{bmatrix} 1 \\ \mathbf{i} \\ \mathbf{j} \\ \mathbf{k} \end{bmatrix} \tag{2.40}$$

where $\mathbf{i}$, $\mathbf{j}$ and $\mathbf{k}$ are imaginary components. Multiplication between quaternion imaginary components are similar to ordinary imaginary multiplication. The multiplication rules for quaternions are given by

$$\begin{array}{lll} \mathbf{i}\cdot\mathbf{i} = -1 & \mathbf{i}\cdot\mathbf{j} = \mathbf{k} & \mathbf{i}\cdot\mathbf{k} = -\mathbf{j} \\ \mathbf{j}\cdot\mathbf{j} = -1 & \mathbf{j}\cdot\mathbf{i} = -\mathbf{k} & \mathbf{j}\cdot\mathbf{k} = \mathbf{i} \\ \mathbf{k}\cdot\mathbf{k} = -1 & \mathbf{k}\cdot\mathbf{i} = \mathbf{j} & \mathbf{k}\cdot\mathbf{j} = -\mathbf{i} \end{array}. \tag{2.41}$$

To specify a vector from a body frame, $\mathbf{r}$ in a NED frame, the components are redefined as the complex components of a quaternion.

$$\mathbf{r} = \mathbf{i}r_1 + \mathbf{j}r_2 + \mathbf{k}r_3 + 0 \tag{2.42}$$

where the scalar is set to zero. Then the rotation is defined as [23]

$$\mathbf{r}^n = \mathbf{q}^*\mathbf{r}^b\mathbf{q}. \tag{2.43}$$

$\mathbf{q}^*$ denotes the complex conjugate of $\mathbf{q}$ and is defined as a negation of all the complex components. For quaternions the complex conjugate is the same as the inverse. The multiplication between two arbitrary quaternions is defined as

$$\begin{aligned}\mathbf{q}\cdot\mathbf{p} =&(q_0+q_1\mathbf{i}+q_2\mathbf{j}+q_3\mathbf{k})\cdot(p_0+p_1\mathbf{i}+p_2\mathbf{j}+p_3\mathbf{k})\\ =&(q_0p_0-q_1p_1-q_2p_2-q_3p_3)+(q_0p_1+q_1p_0+q_2p_3-q_3p_2)\mathbf{i}\\ &+(q_0p_2-q_1p_3+q_2p_0+q_3+p_1)\mathbf{j}+(q_0p_3+q_1p_2-q_2p_1+q_3p_0)\mathbf{k}\\ =&\begin{bmatrix}q_0 & -q_1 & -q_2 & -q_3\\ q_1 & q_0 & -q_3 & q_2\\ q_2 & q_3 & q_0 & -q_1\\ q_3 & -q_2 & q_1 & q_0\end{bmatrix}\begin{bmatrix}p_0\\ p_1\\ p_2\\ p_3\end{bmatrix}.\end{aligned} \tag{2.44}$$

Expanding (2.43) according to (2.44) gives the equation:

$$\mathbf{r}^n=\begin{bmatrix}0 & 0\\ 0 & C\end{bmatrix}\mathbf{r}^b \tag{2.45}$$

C is the rotation matrix, derived in [23], used to rotate a vector between different frames and is equivalent to the Direction cosine matrix. The difference is what the individual elements represents and how they propagate.

$$C=\begin{bmatrix}q_0^2+q_1^2-q_2^2-q_3^2 & 2(q_1q_2+q_0q_3) & 2(q_1q_3-q_0q_2)\\ 2(q_1q_2-q_0q_3) & q_0^2-q_1^2+q_2^2-q_3^2 & 2(q_2q_3+q_0q_1\\ 2(q_1q_3+q_0q_2) & 2(q_2q_3-q_0q_1) & q_0^2-q_1^2-q_2^2+q_3^2\end{bmatrix} \tag{2.46}$$

Propagation of quaternions

The change rate of the quaternion rotation matrix [22] is given by:

$$\dot{\mathbf{q}}=0.5\mathbf{q}\cdot\mathbf{p}_{nb}^b \tag{2.47}$$

where

$$\mathbf{p}_{nb}^b=\begin{bmatrix}0\\ \omega_x^b\\ \omega_y^b\\ \omega_z^b\end{bmatrix} \tag{2.48}$$

and ω_i^b is the rotation rates in the body frame. Expanding this equation according to (2.41) gives

$$\begin{bmatrix}\dot{q_1}\\ \dot{q_2}\\ \dot{q_3}\\ \dot{q_4}\end{bmatrix}=0.5\begin{bmatrix}q_0 & -q_1 & -q_2 & -q_3\\ q_1 & q_0 & -q_3 & q_2\\ q_2 & q_3 & q_0 & -q_1\\ q_3 & -q_2 & q_1 & q_0]\end{bmatrix}\begin{bmatrix}0\\ \omega_x\\ \omega_y\\ \omega_z\end{bmatrix}. \tag{2.49}$$

This can be rewritten as

$$\begin{pmatrix}0 & -\omega_x & -\omega_y & -\omega_z\\ \omega_x & 0 & \omega_z & -\omega_y\\ \omega_y & -\omega_z & 0 & \omega_x\\ \omega_z & \omega_y & -\omega_x & 0\end{pmatrix}\begin{pmatrix}q_0\\ q_1\\ q_2\\ q_3\end{pmatrix}=\begin{pmatrix}-q_1 & -q_2 & -q_3\\ q_0 & -q_3 & q_2\\ q_3 & q_0 & -q_1\\ -q_2 & q_1 & q_0\end{pmatrix}\begin{pmatrix}\omega_x\\ \omega_y\\ \omega_z\end{pmatrix}. \tag{2.50}$$

For further use, the following expressions are defined,

$$\dot{\mathbf{q}} = \frac{1}{2} S(\omega)\mathbf{q}, \qquad \dot{\mathbf{q}} = \frac{1}{2} \bar{S}(\mathbf{q})\omega \tag{2.51}$$

where,

$$S(\omega) = \begin{pmatrix} 0 & -\omega_x & -\omega_y & -\omega_z \\ \omega_x & 0 & \omega_z & -\omega_y \\ \omega_y & -\omega_z & 0 & \omega_x \\ \omega_z & \omega_y & -\omega_x & 0 \end{pmatrix} \tag{2.52}$$

$$\bar{S}(\mathbf{q}) = \begin{pmatrix} -q_1 & -q_2 & -q_3 \\ q_0 & -q_3 & q_2 \\ q_3 & q_0 & -q_1 \\ -q_2 & q_1 & q_0 \end{pmatrix}. \tag{2.53}$$

Chapter 3

Sensors

The sensors on EasyPilot belong to the MEMS technology. MEMS stands for *Micro-Electro-Mechanical Systems*, and it consists of extremely small sensor elements between 0.02[mm] and 1[mm] together with a processing unit. This type of sensor is common in a strapdown system, where all the sensors are fixed on a chip. This is also the case for EasyPilot.

3.1 Gyroscopes

MEMS gyroscopes measures rotation rate around fixed axes. These are used in various applications due to their low cost. The autopilot is equipped with a 3-axis analog MEMS gyroscope which measures the roll-rate, pitch-rate and yaw-rate. Gyroscopes are useful from many aspects, they can be integrated to acquire orientation or the rotation rates can be used to suppress external disturbances. The analog sensors are sampled by the processor at approximately 200Hz. When logging from the autopilot, limitations in transfer rates set the sample rate to 120Hz. The gyroscopes bandwidth is higher than this and therefore the Nyquist criteria is not fulfilled, thus yielding limitations in frequency analysis.

3.1.1 Performance

There are several factors to consider when evaluating a gyroscope [1], such as

Scale factors - Since it is an analog sensor the measured voltage from the sensor must be scaled to rotation rate. This number is often given by the manufacturer, but it may vary between components. This factor can also be dependent on temperatures and accelerations.

Non-linearity of scale factors - The scaling factor is not necessarily a constant, it may differ between different rotation rates.

Alignment errors - The axes of the sensor can be non-orthogonal. This means that if we rotate the sensor around one of its axes, another axis will sense the rotation as well.

Bias - If the sensor is laying still and if it has not got zero mean on all axes, a bias is present.

Bias and scaling stability - The bias and scaling factor are not always constant over time.

Random drift rate - The noise on the sensor output is often analyzed in terms of Allan variance [2, 25]. This is however not presented here due to the fact that the bandwidth of the gyroscopes is higher than the sample rate, which means that the Nyquist criteria is not fulfilled.

These types of errors can be compensated for by calibration. But there are other performance factors that are sensor specific such as resolution, bandwidth, turn-on time and shock resistance. To get a good calibration that takes all errors into account, reliable measurement equipment is needed. During this master thesis no such equipment is available. Because of this, the only errors that will be calibrated for are bias and a constant scaling factor. The change in bias that may occur will be handled by filtering and is described in Chapter 4 and 5.

3.1.2 Statistical analysis

Most information about the gyroscopes can be gathered by collecting data when the sensor is placed at stand-still. In this section bias and noise levels will be analyzed and compared to the sensor datasheet.

In Figure 3.1, measurements from the 3-axis gyroscope is plotted. From this dataset we can derive bias and variance. Due to limitations in communication the gyroscopes are sampled at approximately $120Hz$. The bias is computed simply by taking the mean of each sensor. The biases for the gyroscopes are presented in the table below.

Gyroscope	Bias $[rad/s]$
Roll	-0.1069
Pitch	-0.1268
Yaw	-0.0192

The typical rate noise density of the gyroscopes from the datasheet is given in $^\circ/s/\sqrt{Hz}$. These are calculated from the same dataset as the biases above. The rate noise density and variance for the gyroscopes used are given in the table below.

Gyroscope	Rate noise density $[^\circ/s/\sqrt{Hz}]$	Variance $[rad^2/s^2]$
According to manufacturer	0.035	–
Roll	0.0873	$2.84e-4$
Pitch	0.1231	$5.65e-4$
Yaw	0.0390	$5.66e-5$

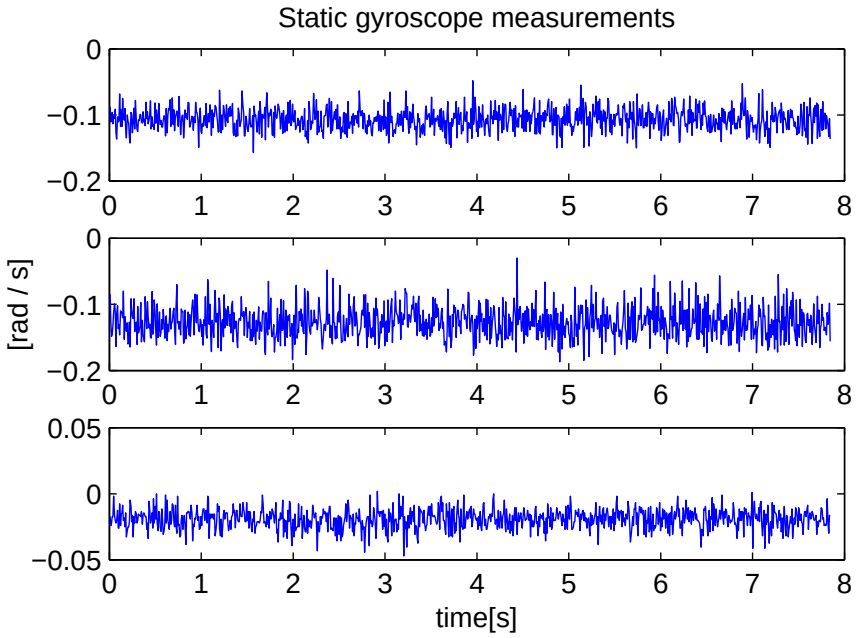

Figure 3.1. Gyrscope measurements in [rad/s] from all three gyros, roll, pitch and yaw.

Even though the noise rate densities from the measurements are higher than the typical rate noise density from the datasheet, this is not interpreted as a malfunctioning gyroscope. The typical values are given assuming that the gyroscope is mounted at an ideal position, that the input voltage is good and that there are no external disturbances. The EasyPilot is however not an ideal mounting position since there are a lot of components causing local disturbances in power supply and inducing currents in the gyroscope circuit.

3.1.3 Calibration

The gyroscopes are calibrated for bias and scaling. The output voltage, U from the gyroscope is translated to an angular rate according to

$$\omega = (U - b^U) \cdot k \tag{3.1}$$

where b^U is the bias in voltage and k is the scaling factor. The bias factor can be identified by sampling the gyroscopes when they are lying still with good precision. To get a good calibration on the scaling factor, a precise known rotation is needed around a single axis. When using the gyroscopes together with a filter that uses accelerometer and magnetometer, the scaling factor is not crucial. If a rotation of 90° is performed and the gyroscope is integrated to 85°, the accelerometer and magnetometer will cause the orientation to converge to its correct value. This is described in Chapter 5. In this case the calibration algorithm proposed in Algorithm 1 may be sufficient.

Algorithm 1 Gyroscope calibration

1. **Sample the gyroscope when it is lying still**
2. **Calculate bias:**

   For measurement m_i, i = 1,2,...,M,

   $b^U = \frac{1}{M} \sum_{i=1}^{M} m_i$
3. **Set** $k_{\mathbf{old}} = 1$
4. **Sample the gyroscope when rotating 360 degrees around its axis**
5. **Calculate the scaling:**

   For measurement m_i, i= 1,2,...,M, and sampling time T_s

   $k_{\text{new}} = 2\pi / \left(T_s k_{\text{old}} \sum_{i=1}^{M} m_i \right)$
6. **Set** $k_{\mathbf{old}} = k_{\mathbf{new}} \cdot k_{\mathbf{old}}$ **Repeat from (4) until** $k_{\mathbf{new}} = 1$**.**
7. **Repeat from (1) for all gyroscope axes.**

3.2 Accelerometer

An accelerometer measures proper acceleration, that is weight per unit of a test mass. This means that the actual gravity of the earth is measured as well as accelerations due to motion. Since the gravity vector is known, the accelerometer can be used to estimate both orientation and acceleration. It is however impossible to distinguish acceleration from orientation if neither is known. The accelerometer used in EasyPilot is an analog 3-axis MEMS accelerometer.

3.2.1 Performance

The performance of an accelerometer can be evaluated in roughly the same way as the gyroscopes. They are both of MEMS technology and will therefore have the same errors related to MEMS construction. While the accelerometer can be used to gain long-term stability in orientation, it will only have short term stability in navigation since the position is a double integration. This can be illustrated by solving the following integral,

$$v = \int_0^t a(t) + b \, \mathrm{d}t = \int_0^t a(t) \, \mathrm{d}t + bt \tag{3.2}$$

where the integral over $a(t)$ is the true velocity and bt is the integrated bias error. A second integral solving the position will cause the bias error to be even larger. And over time, the term bt will be very significant.

More performance criteria and how to measure them are described in Chapter 8 in [21]

3.2.2 Statistical analysis

In Figure 3.2 the accelerometer is sampled at 120Hz at stand-still flat oriented, which means that the z-axis accelerometer should measure one negative g in mean and the x- and y-axis should have zero mean. The bias on the x- and y-axis can be derived by just taking the mean of the measurements. The z-axis accelerometer measures the gravity vector which needs to be taken into account. The bias of the z-axis for N measurements, m_z, becomes

$$b_z = \frac{1}{N} \sum_{k=1}^{N} (m_z + g). \tag{3.3}$$

In the table below the accelerometer biases are presented.

Accelerometer	$[g]$
x-axis	-0.0475
y-axis	0.0562
z-axis	-0.0406

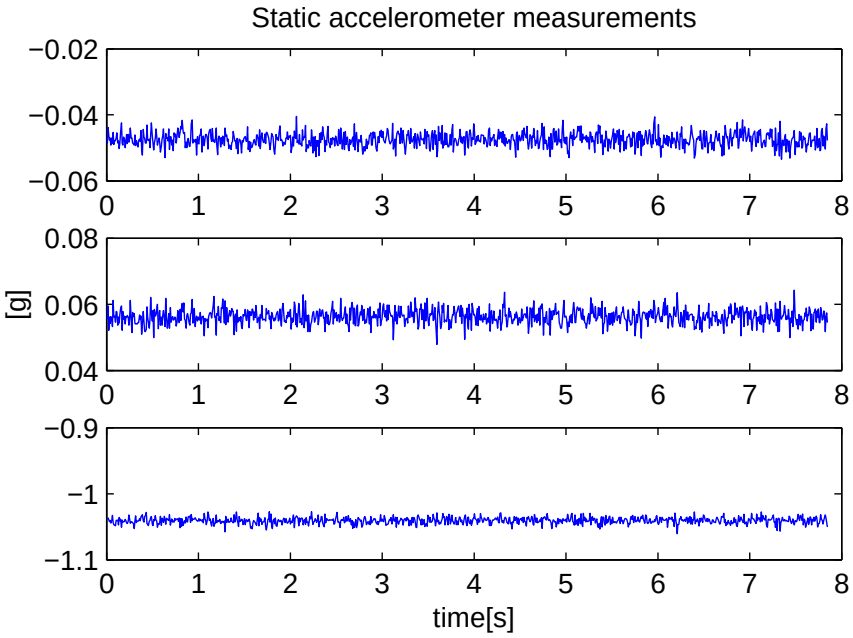

Figure 3.2. Accelerometers measuring acceleration in unit [g]. From top, x-axis, y-axis and z-axis. The accelerometer is laying flat and is not calibrated.

When performing measurements for estimation of accelerometer bias the orientation of the sensor is of importance. If the sensor is tilted some degrees the x- or y-axis sensors will measure a small part of the gravity. This must not be interpreted as a sensor bias.

The noise performance on the sensor is given by the manufacturer is $\mu g/\sqrt{Hz}$. From the dataset presented in Figure 3.2, the mean is removed and noise density is calculated. The noise ratios of the sensor together with typical values from manufacturer are presented in the table below.

Accelerometer	Noise density $\mu g/\sqrt{Hz}$	Manufacturer typical value $\mu g/\sqrt{Hz}$
x-axis	193.92	150
y-axis	207.62	150
z-axis	454.60	300

Here, the noise ratios are higher than the manufacturers typical values. Since the gyroscopes showed the same result this is probably due to external disturbances as discussed in Section 3.1.2.

3.2.3 Calibration

Some of the errors in the sensor can be calibrated for. In this report a calibration algorithm that is compensating for scaling errors and bias in the individual axes

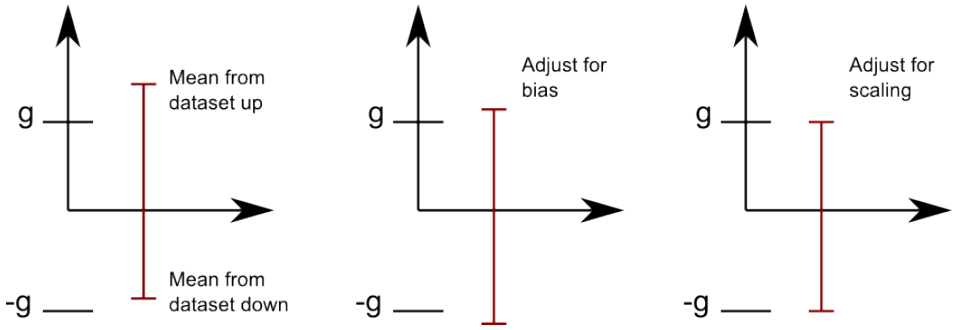

Figure 3.3. An illustration of the accelerometer calibration as given in Algorithm 2.

are presented in Algorithm 2. An illustration of the calibration algorithm can be seen in Figure 3.3.

Algorithm 2 Accelerometer calibration

1. **Collect M_1 samples $m_{1,i}$ of accelerometer with an axis aligned with the direction of gravity**

2. **Collect M_2 samples $m_{2,i}$ of accelerometer with the same axis aligned with the opposite direction of gravity**

3. **Calculate the off-set b_a according to**

$$b_a = \frac{1}{2}\left(\frac{1}{M_1}\sum_{i=1}^{M_1} m_{1,i} + \frac{1}{M_2}\sum_{i=1}^{M_2} m_{2,i}\right)$$

4. **Calculate the scaling factor according to**

$$k = 1/\left(\frac{1}{M_1}\sum_{i=1}^{M_1} m_{1,i} - b_a\right)$$

5. **Repeat from step (1) on all accelerometer axes.**

Sometimes the accelerometer axes may be misaligned, non-orthogonal. If the misalignment is significant, or if it is of great importance that no misalignment exists, this can also be calibrated for. An algorithm for this is presented in [19].

3.3 Magnetometer

In avionics a magnetometer is often used to calculate heading of the vessel. The heading can be calculated by measuring the strength and direction of the magnetic

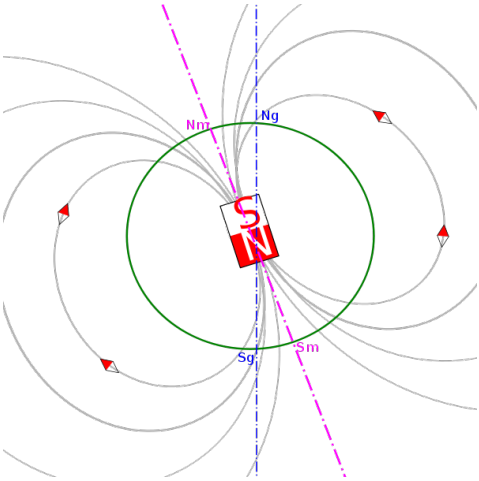

Figure 3.4. A 2D projection of the earth's magnetic field.

field since the earth's magnetic field is known. The field strength is measured in Weber per square meter (Wb/m^2), which is the same as Tesla (T), or in Gauss (G) where,

$$1[G] = 0.0001[T]. \tag{3.4}$$

The earth's magnetic field, even though it is known, is very small (from $0.3G$ in South Africa to $0.6G$ near the poles). This means that the sensor will be very sensitive to disturbance fields, such as electric motors, high voltage wires, hard iron materials etc. The earth's magnetic field can be seen in a 2D projection in Figure 3.4. Here it can be seen that the angle between the surface and the magnetic field increases as we get closer to the magnetic poles, this is called inclination or dip. The same Figure also illustrates the deviation between the geographic north and magnetic north. The angle between magnetic north component and the geographic is called the declination. In Linköping the declination is approximately 4 degrees and the inclination 70 degrees. This will result in larger uncertainties in heading estimation since the magnetic component in the horizontal plane is small relative to the component in the vertical plane.

The EasyPilot is equipped with a tri-axis *anisotropic magnetoresistive* (AMR) magnetometer. This type of magnetometer is very small and is often used in strapdown applications. In the NED frame the earth's magnetic field can be separated into three components. In Linkȹping these are given by

Component	Value
North	15.741 [μT]
East	1.1304 [μT]
Down	48.422 [μT]

In the NED frame this will look like in Figure 3.5. The magnetometer itself will measure a rotation of this vector depending on its orientation.

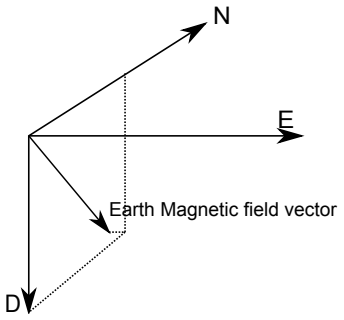

Figure 3.5. The earth's magnetic field in Linköping relative to a NED frame.

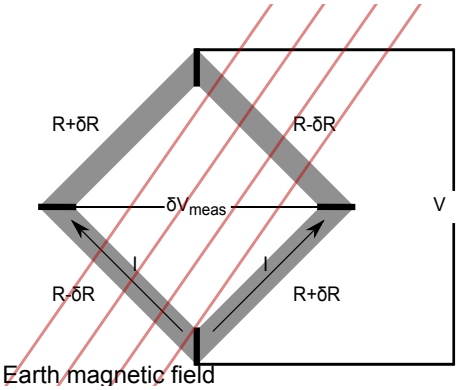

Figure 3.6. Illustration of one of the three wheatstone bridges in an AMR magnetometer.

3.3.1 Anisotropic Magnetoresistive elements

The AMR sensor is constructed by three orthogonally placed magnetic field sensors. Each sensor consists of four magnetoresistive elements that are mounted in a square, a so-called wheatstone bridge. A voltage is applied over two opposite corners of the square and the output voltage is measured over the two others, see Figure 3.6. That means that the measured output should be half of the applied voltage. Due to magnetic interference from external magnetic fields the resistance of the elements in the wheatstone bridge will change, thus changing the output voltage. This change in output voltage is used to calculate the magnetic field strength [16]. In a tri-axis AMR there are three orthogonally placed wheatstone bridges which allow the sensor to sense a magnetic field in three dimensions.

3.3.2 Measurement errors

There are two types of errors that have to be considered to be able to get good readings from the sensors, manufacturing errors and environmental errors. Some

of these are constant for each sensor and some vary for different environments. The next section will describe how these effects are being accounted for. The effects mentioned below are thoroughly described in [16].

Wheatstone bridge alignment errors

When calculating the magnetic field we use the fact that the output voltage from the wheatstone bridge is half of the applied voltage. When an external magnetic field is applied the resistance in the circuit will change. But to get an expected reading of the output voltages from the tri-axis AMR it is required that the wheatstone bridges are exactly orthogonal to each other. Due to manufacturing errors, they are not. This misalignment is constant and sensor specific and does not vary over time.

Element sensitivity errors

The elements in the AMR are not linear in respect to applied magnetic field. A calibration in an environment where the magnetic field strength is $0.6G$ is not valid in an environment where it is $0.4G$. But since the sensor are to be used in a known environment there is only a scale factor between output voltage and magnetic field. This scale factor would not be valid if the AMR is put in a different environment where the strength of the magnetic field is not the same for which the scale factor was derived.

Element magnetization errors

Over time the elements in the AMR will be magnetized. This will result in a change of the sensor's sensitivity axis. This effect is often referred to as cross axis sensitivity errors. If the environment provides a constant magnetic field the norm of the measured magnetic field would be constant. But when the sensitivity axis of the individual elements of the wheatstone bridge differs, this will not be the case. This will result in an illusion that the magnetic field strength of the surroundings change due to the magnetometers orientation.

Hard iron errors

Hard iron errors have nothing to do with the sensor itself, but rather the platform it is mounted on. Hard iron effects are defined by a magnetic source with a constant magnetic field, independent of the platform's orientation. This will cause a perturbation of the magnetic field which will manifest itself as a bias in the sensor readings. An example of this is if the magnetometer is mounted near a wire delivering current. The wire's orientation relative to the magnetometer will never change which means that the disturbance caused by it will be constant.

Soft iron errors

Soft iron deviations are of a more complex nature. These are caused by ferromagnetic materials that are excited by the earth's magnetic field. Because of this, the

magnetic field disturbance will change with the platforms orientation.

3.3.3 Calibration

When calibrating the magnetometer a compensation for all the effects described in Section 3.3.2 will be done. Due to the hard and soft iron errors the calibration must be done when the sensor is mounted on the desired platform. A measurement model including all the errors that are to be compensated for is derived, then a least squares method [11] is used to estimate the parameters.

Measurement model

If only measurement errors are taken into account the model would look like

$$\hat{\mathbf{h}} = \mathbf{h_s} + \boldsymbol{\epsilon} \tag{3.5}$$

where

$$\begin{aligned} \hat{\mathbf{h}} &- \text{ Measured magnetic field} \\ \mathbf{h_s} &- \text{Sensor indicated magnetic field} \\ \boldsymbol{\epsilon} &- \text{Measurement noise} \end{aligned}$$

The sensor indicated magnetic field is however not the same as the earth magnetic field. The hard iron effects can be compensated with a bias term according to,

$$\mathbf{b_{hi}} = [b_{hi_x} \; b_{hi_x} \; b_{hi_x}]^T . \tag{3.6}$$

The effects of soft iron changes the direction of and strength of the sensed field in respect to how the platform is oriented relative to the earth's magnetic field. This effect can be modeled by a scaling of the true field with a 3 by 3 matrix,

$$\mathbf{A_{si}} = \begin{bmatrix} a_{11} & a_{12} & a_{13} \\ a_{21} & a_{22} & a_{23} \\ a_{31} & a_{32} & a_{33} \end{bmatrix} \tag{3.7}$$

This means that the field that the sensor is actually measuring is

$$\mathbf{h} = \mathbf{A_{si}}(\mathbf{h_e} - \mathbf{b_{hi}}) \tag{3.8}$$

What is left is to compensate for the measurement errors in the actual sensor. As depicted in Section 3.3.2, we must compensate for the wheatstone bridge misalignments and the scaling of the current magnetic field. The misalignments are compensated for by multiplying the measurement with a 3 by 3 matrix that projects the measurements on the orthogonal frame on which the sensor is mounted. The scaling of the current magnetic field is compensated for by multiplying the measurements with a 3 by 3 diagonal matrix and the bias is subtracted from the

measurement. The following compensation factors are introduced:

$$\mathbf{M} = \begin{bmatrix} m_{11} & m_{12} & m_{13} \\ m_{21} & m_{22} & m_{23} \\ m_{31} & m_{32} & m_{33} \end{bmatrix} \quad \text{non-orthogonality compensation}$$

$$\mathbf{S} = \begin{bmatrix} s_{11} & 0 & 0 \\ 0 & s_{22} & 0 \\ 0 & 0 & s_{33} \end{bmatrix} \quad \text{scaling compensation}$$

$$\mathbf{b_s} = [b_{s_x}\ b_{s_x}\ b_{s_x}]^T \quad \text{sensor bias compensation}$$

This yields the measurement equation

$$\hat{\mathbf{h}} = \mathbf{SM}(\mathbf{A_{si}}\mathbf{h_e} + \mathbf{b_{hi}}) + \mathbf{b_s} + \boldsymbol{\epsilon} \tag{3.9}$$

where $\hat{\mathbf{h}}$ is the measured field and $\mathbf{h_e}$ is the earth's magnetic field in the frame of the sensor and $\boldsymbol{\epsilon}$ is noise. Although there are a lot of factors affecting the measurement we are not interested in the individual contributions from specific errors, thus introducing:

$$\hat{\mathbf{h}} = \mathbf{A}\mathbf{h_e} + \mathbf{b} + \boldsymbol{\epsilon} \tag{3.10}$$

where,

$$\mathbf{A} = \mathbf{SMA_{si}} \tag{3.11}$$

$$\mathbf{b} = \mathbf{SMb_{hi}} + \mathbf{b_s}. \tag{3.12}$$

Here, $\mathbf{A}$ represents all the scalings and rotations and $\mathbf{b}$ all the biases.

To be able to calculate a vessels orientation we want to know in which direction the earth magnetic field is oriented with respect to the frame of the vessel. From equation (4.28) we can derive the earth magnetic field in the frame that the sensor is mounted,

$$\mathbf{h} = \mathbf{A^{-1}}(\hat{\mathbf{h}} - \mathbf{b} - \boldsymbol{\epsilon}) \tag{3.13}$$

3.3.4 Calibration algorithm using least squares

Equation (3.13) cannot be solved directly using least squares since it is not in quadratic form. But $\mathbf{h}$ is the earth's magnetic field in the frame of the sensor, and under the assumption that the magnitude of the earth's magnetic field is constant the following equation is given:

$$H_m^2 - \mathbf{h^T}\mathbf{h} = 0 \tag{3.14}$$

where H_m is the magnitude of the earth's magnetic field. Substituting $\mathbf{h}$ in equation (3.14) with (3.13) yields the equation

$$(\hat{\mathbf{h}} - \mathbf{b})^{\mathbf{T}}(\mathbf{A^{-1}})^{\mathbf{T}}\mathbf{A^{-1}}(\hat{\mathbf{h}} - \mathbf{b}) - H_m^2 = 0 \tag{3.15}$$

which can be expanded to

$$\hat{\mathbf{h}}(\mathbf{A^{-1}})^{\mathbf{T}}\mathbf{A^{-1}}\hat{\mathbf{h}} - 2(\mathbf{A^{-1}})^{\mathbf{T}}\mathbf{A^{-1}}\mathbf{b}\hat{\mathbf{h}} + \mathbf{b}^{\mathbf{T}}(\mathbf{A^{-1}})^{\mathbf{T}}\mathbf{A^{-1}}\mathbf{b} - H_m^2 = 0. \tag{3.16}$$

This is a quadratic equation according to

$$\hat{\mathbf{h}}^{\mathbf{T}}\mathbf{Q}\hat{\mathbf{h}} + \mathbf{u}^{\mathbf{T}}\hat{\mathbf{h}} + k = 0 \tag{3.17}$$

where

$$\mathbf{Q} = (\mathbf{A}^{-\mathbf{1}})^{\mathbf{T}}\mathbf{A}^{-\mathbf{1}} \tag{3.18}$$
$$\mathbf{u} = -2\mathbf{Q}^{\mathbf{t}}\mathbf{b} \tag{3.19}$$
$$k = \mathbf{b}^{\mathbf{T}}\mathbf{Q}\mathbf{b} - H_m^2 \tag{3.20}$$

$\mathbf{Q}$ is symmetric due to its definition. Thus we can rewrite (3.17) to obtain,

$$0 = \mathbf{y}^T\boldsymbol{\beta} \tag{3.21}$$

where

$$\mathbf{y}^T = \left[(\mathbf{h}\otimes\mathbf{h})^T\ \mathbf{h}^T\ 1\right] \tag{3.22}$$
$$\boldsymbol{\beta} = [Q_{11}\ Q_{12}\ Q_{13}\ Q_{22}\ Q_{23}\ Q_{33}\ u_1\ u_2\ u_3\ k]^T \tag{3.23}$$

where $\otimes$ is the kronecker product. The least squares cost function is defined according to

$$q_{ls}(\boldsymbol{\beta};\mathbf{h}) = (\mathbf{y}^T\boldsymbol{\beta})^2 = \boldsymbol{\beta}^T\mathbf{y}\mathbf{y}^T\boldsymbol{\beta} \tag{3.24}$$

q_{ls} is associated with the cost for one measurement. For solving the least square problem we formulate

$$Q_{ls} = \sum_{l}^{m}\boldsymbol{\beta}^T\mathbf{y}^{(l)}\mathbf{y}^{(l)T}\boldsymbol{\beta} = \boldsymbol{\beta}^T\boldsymbol{\Phi}\boldsymbol{\beta} \tag{3.25}$$

where $\mathbf{y}^{(l)}$ is associated with the l'th measurement. There are several ways of solving the least squares problem defined in (3.25). Here, (3.25) is minimized by setting $\boldsymbol{\beta}\perp\nu_i$, where ν_i is the eigenvector associated with the smallest eigenvalue of $\boldsymbol{\Phi}$. $\boldsymbol{\beta}$ is given by the normalized eigenvector:

$$\boldsymbol{\beta} = \frac{\nu_i}{|\nu_i|} \tag{3.26}$$

$\mathbf{Q}$, $\mathbf{u}$ and k can now be reconstructed from $\boldsymbol{\beta}$, where the lower triangular of Q is set to the upper triangular of Q. The bias term in (3.13) is solved directly by,

$$\mathbf{b} = -\frac{1}{2}\mathbf{Q}^{-1}\mathbf{u}. \tag{3.27}$$

To acquire A^{-1} from (3.13), equation (3.18) can be solved using Cholesky decomposition, giving the complete solution for the magnetometer projection on a sphere,

$$\mathbf{h} = \mathbf{A}^{-\mathbf{1}}(\hat{\mathbf{h}} - \mathbf{b}). \tag{3.28}$$

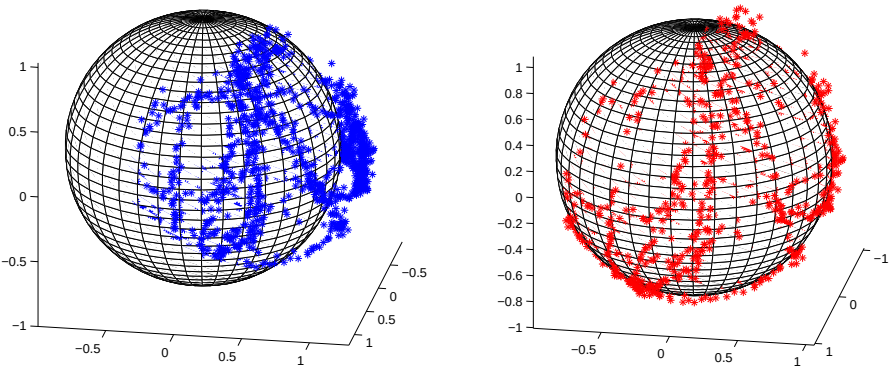

Figure 3.7. To the left is the non-calibrated data with normalized amplitude. To the right is the same data but calibrated.

3.3.5 Calibration results

When calibrating the magnetometer the sensor must be mounted in the same settings as when it is to be used. The magnetometer is fixed to EasyPilot and the EasyPilot is mounted in the aircraft Spy Owl 100. The plane is moved around to collect measurements in various orientations. As seen in the left plot in Figure 3.7, the magnetometer is in need of calibration. In the right plot the same data is calibrated and plotted against the same reference sphere.

3.4 Pressure sensors

In most avionic applications, pressure sensors are used. EasyPilot is equipped with two analog MEMS pressure sensors, one to measure the static pressure and one to measure the stagnation pressure. Stagnation pressure is defined by Bernoulli's equation

$$\textbf{stagnation pressure} = \textbf{static pressure} + \textbf{dynamic pressure}. \tag{3.29}$$

In Figure 3.8 a static source, measuring static pressure, and a pitot tube, measuring stagnation pressure are illustrated for a vessel in motion. When in motion, the air molecules will enter the pitot tubes and press against the inner wall. This will increase the density of air molecules in the pitot tube. But due to the second law of thermodynamics the density will only increase to a certain point, equilibrium. Depending on the speed of the vessel, this equilibrium will correspond to different densities of air in the pitot tube. The stagnation pressure is the pressure measured inside this tube.

The static source is used to measure the pressure surrounding the vessel and the difference between static pressure and stagnation pressure gives dynamic pressure.

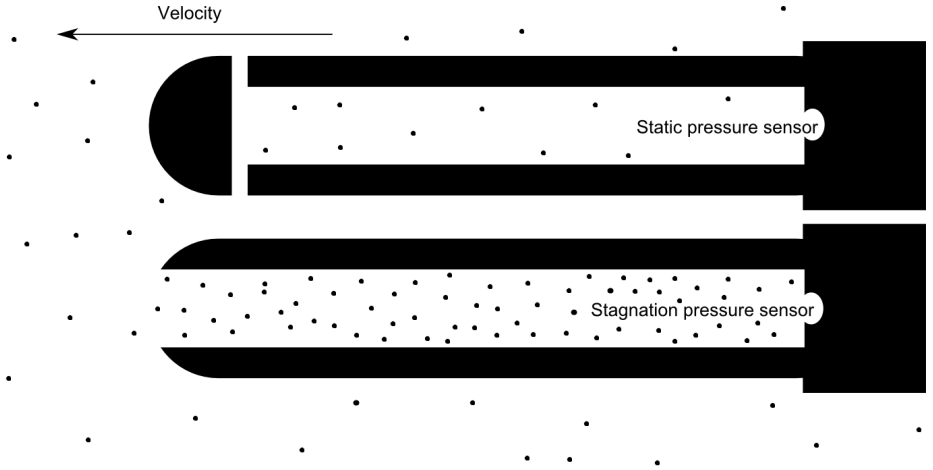

Figure 3.8. The static source (upper) measures static pressure, the pitot tube (lower) measures stagnation pressure. The dots illustrate the density of air molecules.

Knowing the pressure at ground level the height of the vessel can be derived from the static pressure and knowing the dynamic pressure the air speed can be derived. This derivations are described in Section 4.2.5.

3.4.1 Performance

The pressure sensors used are MEMS technology and will have noise and bias. The difference between gyroscopes, accelerometers and magnetometers is that we do not have a constant reference to determine bias from. To be able to bias compensate we must know the exact pressure in the room where we analyse it. But since the air pressure is not constant, the more attractive option is to calibrate an offset, in which the bias is included.

One performance factor that can vary between manufacturers, that is important in Sweden, is the temperature operation interval. Some manufacturers support down to $-40°C$ and some support only down to $0°C$.

3.4.2 Calibration

When the aircraft is standing still on the ground, the stagnation pressure and static pressure should both be the same. In this calibration it is assumed that the ground pressure is equal to the standard atmospheric pressure, $101.325[kPa]$. The calibration of the pressure sensors will therefore only include a bias compensation. The main focus of this calibration is to make sure that the stagnation pressure and static pressure is the same when the aircraft is not moving. If they are not, a false indication of air speed will be persistent.

3.5 GNSS

GNSS, or *Global Navigation Satellite System*, is a navigation system based on satellites with global coverage such as GPS, GLONASS and soon to be operating Galileo. All satellites within a GNSS have synchronized clocks and transmit their clock time regularly. A receiver compares time of arrival from several different satellites and from this information position can be derived. The American GNSS, GPS, was the first GNSS system to become available for civil use in 1983. At this point there were still restrictions for the civil market which were removed in 2000.

There are a lot of receiver manufacturers on the market that treat the signals from the satellites in their own way and they also choose what data to deliver. The manufacturers usually support most of the data specified in the protocol specified by *National marine electronics association*, NMEA, as given in [18]. When using a GNSS in a product the user must rather choose from the variety of settings the manufacturer provides rather than calibrate it. The most common receiver settings and how they affect performance are thoroughly described in [12].

3.5.1 Position estimation

If the receiver clock is synchronized with the satellite clock and the satellite clock emits its current time, the distance from the satellite can be calculated. This is because it will take time for the satellites clock pulse to reach the receiver. The difference in time of arrival and the emitted time stamp can be used to calculate the distance to the satellite according to

$$d = c\Delta t \tag{3.30}$$

where Δt is the difference between time of emitting and time of arrival. In a 2D example this means that the receiver must be located on the circle with radius d, 3.9. Since we know that we must be located on the earth (on the circumference of the 2D circle) there are only two possible positions to be at, see Figure 3.9. In the same Figure another satellite is added, which eliminates one of the possibilities, thus yielding the true position of the receiver.

In the real world we have three dimensions, which means that we must add one extra satellite to be able to determine a position. Also, the satellites have synchronized atomic clocks which the receiver has not. The unknown time brings an extra dimension in to the problem and therefore four satellites are required to determine the position in a GNSS [27].

3.5.2 Speed and direction estimation

Although many receivers use extensive filtering from positioning to acquire speed, modern devices may also track the frequencies of the satellite signals and estimate speed using the Doppler effect [5]. The Doppler effect is illustrated in Figure 3.10. This principle is based on the experienced wavelength of GPS signals. If a receiver is moving towards a satellite, the wavelength will be experienced as shorter than if the receiver was moving away from it.

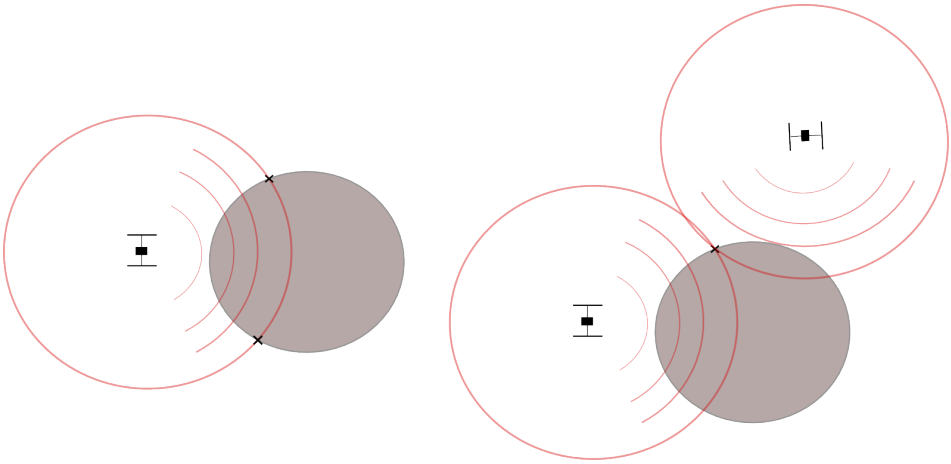

Figure 3.9. Illustration of GNSS positioning principle in 2D.

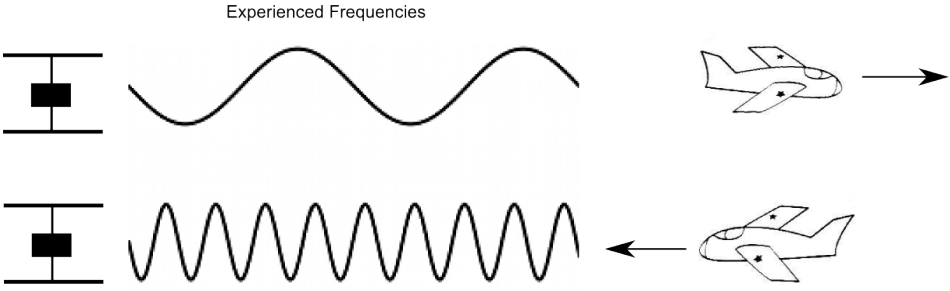

Figure 3.10. The principle of determining speed using the Doppler effect. When the plane moves away from the satellites the experienced frequency of the GPS signal seems lower than if it is moving towards it.

Chapter 4

Modelling

In systems like the autopilot, the measurements given by the sensors themselves are not what is interesting. In most cases we want to know information about the system that has sensors mounted on it. If we want to know how a plane is side slipping in the wind, there is no sensor to measure this. Therefore, we must relate what we can measure to what we want to know.

A measurement model is a mathematical description of what is being measured. This can be exemplified by a gyroscope that measures rotation rate in $[rad/s]$. A simple measurement model relating the measurement to $[^\circ/s]$ can then be stated as

$$y = \frac{\pi}{180}\theta \tag{4.1}$$

where y is the measurement given in $[rad/s]$ by the gyroscope and θ is rotation rate given in $[^\circ/s]$.

Virtual measurements can also be created in a similar way. If it is required to have a measurement in $[^\circ/s]$, equation (4.1) can be arranged to

$$y' = \frac{180y}{\pi}. \tag{4.2}$$

This type of manipulation of measurement equation is a simple way of extracting information. It can however cause problems since we will always manipulate the noise of the sensors as well. In reality, what is being measured by the gyroscope is

$$y = \frac{\pi}{180}\theta + v \tag{4.3}$$

where v is measurement noise. When the measurement equation is rearranged, the true result becomes

$$y' = \frac{180}{\pi}\left(\frac{\pi}{180}\theta + v\right) = \theta + \frac{180}{\theta}v. \tag{4.4}$$

Filters like the Extended Kalman filter do not require manipulation of the measurement equations. The measurement equation is derived so that the measurement is a function of states included in the filter. This gives the possibility to

add measurements that measures a mixture of states. For example, if a sensor is measuring wind speed a simple measurement equation could look like

$$y = v^{\text{ground}} + v^{\text{wind}}. \tag{4.5}$$

If v^{ground} and v^{wind} are included as states in an Extended Kalman filter, this measurement can be used as a measurement equation without manipulation.

In the Extended Kalman filter case a model over the system is derived according to

$$\dot{\mathbf{x}} = f(\mathbf{x}) \tag{4.6}$$
$$\mathbf{y} = g(\mathbf{x}) + \mathbf{v}. \tag{4.7}$$

Here, $\mathbf{x}$ is the state of the Extended Kalman filter, f is the function describing the system dynamics, $\mathbf{y}$ is the measurements, g is the equation relating the measurements to the system states and $\mathbf{v}$ is the measurement noise.

Each section in this chapter describes required models for a certain type of filter. First system models are presented to give an overview of what is to be estimated. Then the measurement models or virtual measurements that relates the system models to the measurements are presented.

4.1 Height estimation model

The height can be described as a function of pressure, and is derived in [26],

$$h = K \log\left(\frac{P_{s0}}{P_s}\right) + h_0 \tag{4.8}$$

where h_0 is the height at ground level, P_{s0} is the static pressure at ground level and K is a parameter that depends on temperature.

We can rearrange (4.8) to acquire

$$h - h_0 = K\left(\log(P_{s0}) - \log(P_s)\right) = \begin{bmatrix} 1 & -\log P_s \end{bmatrix} \begin{bmatrix} K\log(P_{s0}) \\ K \end{bmatrix} \tag{4.9}$$

We now have an equation on the form

$$y = \psi^T \theta \tag{4.10}$$

where

$$\psi = \begin{bmatrix} 1 \\ -\log(P_s) \end{bmatrix}, \quad \theta = \begin{bmatrix} K\log(P_{s0}) \\ K \end{bmatrix}. \tag{4.11}$$

This model is derived under the assumption that the current pressure, P_s, is a known parameter. The model proposed here is designed so that a parameter estimation using RLS, *Recursive Least Squares*, with exponential forgetting factor can be utilized to estimate K in real-time. The RLS algorithm is described in

Section 5.2 The drawback with this method is that the pressure at ground level can change, for example due to an incoming low pressure area.

The reason this model is proposed for use together with RLS is due to the difficulty of performing a calibration, providing K and P_{s0}. It is more appropriate utilizing information from the GPS to estimate K in real-time, after P_{s0} and h_0 has been set as constants at ground.

4.2 INS state space models

An INS, *Inertial Navigation System*, is a system that calculates position, velocity and orientation. With the given sensors for EasyPilot, the following four models are presented with no input signals. The position is defined in Longitude-Latitude, the velocities and accelerations are described in the NED frame and the quaternions represent a rotation from a body frame to the NED frame.

The models proposed only includes kinematic relationships between states due to the fact that the autopilot is to be used in many different air frames. If the autopilot where to be used in a specific airframe, a model over the system could have been derived. This would of course result in higher complexity, but most likely you could expect better performance.

Model 1

The states we want to estimate is the position, $\mathbf{p}$, velocities, $\mathbf{v}$, and the orientation, $\mathbf{q}$. The sensors that we want to utilize are gyroscopes, accelerometers, magnetometers and GPS. If we want to use the accelerometer, which measures the gravity vector as well as acceleration, we must include states for acceleration. The accelerometer also has biases, which is why we must add states for this as well. The gyroscopes measures change in orientation which can be used as an input, or as in this case, added as states. The gyroscopes will also measure a bias which must be included as separate states. The GPS measures velocities and the magnetometer measures the magnetic field. Other effects that these sensors might have are disregarded. It is important to decide what effects to include in a state space model to make the best use of available sensors. For example, the magnetometer has bias to and the accelerometers and gyroscopes has scaling factors that may vary. But if to many effects are added, without additional sensors, the model will be non observable.

This model can be studied further in [8] and is given by:

$$\begin{pmatrix} \dot{\mathbf{p}} \\ \dot{\mathbf{v}} \\ \dot{\mathbf{a}} \\ \dot{\mathbf{q}} \\ \dot{\boldsymbol{\omega}} \\ \dot{\mathbf{b}}^{\mathbf{acc}} \\ \dot{\mathbf{b}}^{\mathbf{gyro}} \end{pmatrix} = \begin{pmatrix} 0 & P(\mathbf{p}) & 0 & 0 & 0 & 0 & 0 \\ 0 & 0 & I & 0 & 0 & 0 & 0 \\ 0 & 0 & 0 & 0 & 0 & 0 & 0 \\ 0 & 0 & 0 & 0 & S(\boldsymbol{\omega})/2 & 0 & 0 \\ 0 & 0 & 0 & 0 & 0 & 0 & 0 \\ 0 & 0 & 0 & 0 & 0 & 0 & 0 \\ 0 & 0 & 0 & 0 & 0 & 0 & 0 \end{pmatrix} \begin{pmatrix} \mathbf{p} \\ \mathbf{v} \\ \mathbf{a} \\ \mathbf{q} \\ \boldsymbol{\omega} \\ \mathbf{b}^{\mathbf{acc}} \\ \mathbf{b}^{\mathbf{gyro}} \end{pmatrix} + \begin{pmatrix} 0 & 0 & 0 & 0 \\ 0 & 0 & 0 & 0 \\ I & 0 & 0 & 0 \\ 0 & 0 & 0 & 0 \\ 0 & I & 0 & 0 \\ 0 & 0 & I & 0 \\ 0 & 0 & 0 & I \end{pmatrix} \begin{pmatrix} v^a \\ v^\omega \\ v^{b,a} \\ v^{b,\omega}. \end{pmatrix} \tag{4.12}$$

$S(\boldsymbol{\omega})$ is defined in (2.52) and $P(\mathbf{p})$ is the relationship between NED velocities and position given by WGS84 as defined in (2.11) and (2.12). These are non-linear functions, and this is therefore not a proper state space model. To make an approximation of a state space model, $S(\boldsymbol{\omega})$ and $P(\mathbf{p})$ must be linearized. This can be seen in Appendix A.

Model 2

The second proposed model includes all states as Model 1 to make use of gyroscopes, accelerometers, magnetometer and GPS. In addition to these sensors, measurements from pitot tubes are to be added. The pitot tube measures the sum of airspeed and ground speed, hence we must add states for the wind to allow this measurement.

Model 1 is augmented with the following states,

$$w = \begin{pmatrix} w_N \\ w_E \end{pmatrix} \tag{4.13}$$

where the wind has a strength defined in north and east respectively. The second

model is then formed according to:

$$\begin{pmatrix} \dot{\mathbf{p}} \\ \dot{\mathbf{v}} \\ \dot{\mathbf{a}} \\ \dot{\mathbf{q}} \\ \dot{\boldsymbol{\omega}} \\ \dot{\mathbf{b}}^{\mathbf{acc}} \\ \dot{\mathbf{b}}^{\mathbf{gyro}} \\ \dot{\mathbf{w}} \end{pmatrix} = \begin{pmatrix} 0 & P(\mathbf{p}) & 0 & 0 & 0 & 0 & 0 & 0 \\ 0 & 0 & I & 0 & 0 & 0 & 0 & 0 \\ 0 & 0 & 0 & 0 & 0 & 0 & 0 & 0 \\ 0 & 0 & 0 & 0 & S(\boldsymbol{\omega})/2 & 0 & 0 & 0 \\ 0 & 0 & 0 & 0 & 0 & 0 & 0 & 0 \\ 0 & 0 & 0 & 0 & 0 & 0 & 0 & 0 \\ 0 & 0 & 0 & 0 & 0 & 0 & 0 & 0 \\ 0 & 0 & 0 & 0 & 0 & 0 & 0 & 0 \end{pmatrix} \begin{pmatrix} \mathbf{p} \\ \mathbf{v} \\ \mathbf{a} \\ \mathbf{q} \\ \boldsymbol{\omega} \\ \mathbf{b}^{\mathbf{acc}} \\ \mathbf{b}^{\mathbf{gyro}} \\ \mathbf{w} \end{pmatrix} + \begin{pmatrix} 0 & 0 & 0 & 0 & 0 \\ 0 & 0 & 0 & 0 & 0 \\ I & 0 & 0 & 0 & 0 \\ 0 & 0 & 0 & 0 & 0 \\ 0 & I & 0 & 0 & 0 \\ 0 & 0 & I & 0 & 0 \\ 0 & 0 & 0 & I & 0 \\ 0 & 0 & 0 & 0 & I \end{pmatrix} \begin{pmatrix} v^a \\ v^\omega \\ v^{b,a} \\ v^{b,\omega} \\ v^w \end{pmatrix} \tag{4.14}$$

Model 3

A simpler model can be stated if only the orientation of the plane is of interest. This model can use gyroscope, magnetometer and accelerometer as measurements.

$$\begin{pmatrix} \dot{\mathbf{a}} \\ \dot{\mathbf{q}} \\ \dot{\boldsymbol{\omega}} \\ \dot{\mathbf{b}}^{\mathbf{gyro}} \end{pmatrix} = \begin{pmatrix} 0 & 0 & 0 & 0 \\ 0 & 0 & S(\boldsymbol{\omega})/2 & 0 \\ 0 & 0 & 0 & 0 \\ 0 & 0 & 0 & 0 \end{pmatrix} \begin{pmatrix} \mathbf{a} \\ \mathbf{q} \\ \boldsymbol{\omega} \\ \mathbf{b}^{\mathbf{gyro}} \end{pmatrix} + \begin{pmatrix} I & 0 & 0 \\ 0 & 0 & 0 \\ 0 & I & 0 \\ 0 & 0 & I \end{pmatrix} \begin{pmatrix} v^a \\ v^\omega \\ v^{b,\omega} \end{pmatrix} \tag{4.15}$$

This model includes 13 states which reduces the complexity when applying an Extended Kalman filter to it. Information that would be useful for estimating acceleration in the body is lost. For this model to work a good and reliable magnetometer and a well calibrated accelerometer is a must.

Model 4

Another simple model that only holds states for position, speed, heading and wind speed can be formed according to:

$$\begin{pmatrix} \dot{\mathbf{p}} \\ \dot{\mathbf{v}} \\ \dot{\mathbf{w}} \\ \dot{\theta} \end{pmatrix} = \begin{pmatrix} 0 & P(\mathbf{p}) & 0 & 0 \\ 0 & 0 & 0 & 0 \\ 0 & 0 & 0 & 0 \\ 0 & 0 & 0 & 0 \end{pmatrix} \begin{pmatrix} \mathbf{p} \\ \mathbf{v} \\ \mathbf{w} \\ \theta \end{pmatrix} + \begin{pmatrix} 0 & 0 & 0 \\ I & 0 & 0 \\ 0 & I & 0 \\ 0 & 0 & 1 \end{pmatrix} \begin{pmatrix} v^v \\ v^w \\ v^\theta \end{pmatrix} \tag{4.16}$$

where θ is the heading of the plane.

Usage of this model demands a GPS, pitot tubes and magnetometer. The magnetometer is used to calculate an artificial measurement of the heading. If a model like this is to be used in avionics there must be complementary filters for

estimation of the body's orientation. This can still be useful as an alternative to estimate winds and heading.

4.2.1 Measurement equations

In the previous section, different kinematic models where proposed. It was also discussed briefly why certain states, such as sensor biases, must be included in the state space model. In this section the measurement equations for the proposed models are presented. The measurement equations may be different depending on what state space model they are relating to. Here, the measurement equations proposed relates mainly to Model 1 and Model 2 if not stated otherwise.

4.2.2 Gyroscopes

The gyroscopes measure the rotation rate relative to an external frame, which gives the measurement equation

$$\mathbf{y}^{gyro} = \begin{pmatrix} 1 & 0 & 0 \\ 0 & 1 & 0 \\ 0 & 0 & 1 \end{pmatrix} \begin{pmatrix} \omega_x \\ \omega_y \\ \omega_z \end{pmatrix} + \begin{pmatrix} b^{gyro,x} \\ b^{gyro,y} \\ b^{gyro,z} \end{pmatrix}. \tag{4.17}$$

If the biases are not included in the system model this is not a valid measurement. In that case the measurement would be adjusted as:

$$\mathbf{y}^{gyro'} = \mathbf{y}^{gyro} - \begin{pmatrix} b^{gyro,x} \\ b^{gyro,y} \\ b^{gyro,z} \end{pmatrix} \tag{4.18}$$

This adjusted measurement equation can be used to reduce the system state matrix by 3 dimensions. The big problem with this is that we don't know if the bias is constant which implicates we must calculate it somehow, and when to calculate it is a problem too since we don't know when we are perfectly still. However, if the model is to complex for a certain application the bias states can be removed from the state space model. In this case, a calibration is needed at every start-up to determine biases.

4.2.3 Accelerometers

The accelerometers that are fixed in the body measures accelerations that are applied. These are not the accelerations we are interested in for the models described in Section 4.2. The accelerometer output will therefore be rotated from the NED frame to the body frame, thus the measurement equation

$$\mathbf{y}^{acc} = C_b^n(\mathbf{a} - \mathbf{g}) - \mathbf{b}^{acc} + \mathbf{e}^{\mathbf{acc}} \tag{4.19}$$

where $\mathbf{a}$ is the acceleration on the body in the NED frame. The same reasoning about the bias' in Section 4.2.2 applies here as well.

Measurement of attitude using accelerometers and pitot tubes

If the sensor platform has accelerometers and gyroscopes and pitot tubes it would be hard to estimate the orientation and actual movements simultaneously using an EKF. The reason that this is presented here is that in some airframes, on which the sensor platform is mounted, there is too much magnetic disturbance which makes usage of the magnetometer improper. If this is the case and the GPS signal is lost it is desirable to have a backup filter that can estimate attitude.

First the measurement equation is adjusted. Equation (4.19) is rewritten to:

$$\mathbf{y}^{acc} = C_b^n(-\mathbf{g}) + \mathbf{a}^b - \mathbf{b}^{acc} \tag{4.20}$$

where $\mathbf{a}^b$ is the accelerations in the body frame. The centripetal accelerations experienced in the body is derived in [7] and is estimated by

$$\hat{a}^c = \boldsymbol{\omega} \times (\boldsymbol{\omega} \times \rho \mathbf{r}) \tag{4.21}$$

where $\boldsymbol{\omega}$ is the turn rate, ρ is the curve radius and $\mathbf{r}$ is a unit vector that points to the center of the turn. The tangential speed is then given by

$$v^{tan} = \boldsymbol{\omega} \times \rho \mathbf{r} \tag{4.22}$$

If the angle of attack is α, then the air speed measured by the pitot tube is given by

$$v_{air} = |v_{air}| \begin{pmatrix} \cos\alpha \\ 0 \\ \sin\alpha \end{pmatrix} \tag{4.23}$$

To get an easy calculated approximation, the angle of attack is set to zero in this application thus yielding

$$\hat{a}^c = \boldsymbol{\omega} \times \begin{pmatrix} v_{\text{air}} \\ 0 \end{pmatrix} \tag{4.24}$$

Here $\boldsymbol{\omega}$ is the measurements from the gyroscopes. The ordinary accelerations caused by thrust can be estimated by an Euler forward approximation of the derivatives of the pitot tube measurements. This acceleration is approximated as straight forward,

$$a_x = \frac{v_k - v_{k-1}}{T_s} \tag{4.25}$$

An assumption that no other accelerations exist in the body will give the equation

$$\mathbf{a^b} = \boldsymbol{\omega} \times \begin{pmatrix} v_{\text{air}} \\ 0 \end{pmatrix} + \begin{pmatrix} a_x \\ 0 \\ 0 \end{pmatrix} \tag{4.26}$$

Now an estimate of the rotation can be calculated from

$$\mathbf{y}^{acc} - \mathbf{a}^b = \mathbf{y}^{acc'} = C_b^n \mathbf{g} + \mathbf{e}^{acc} \tag{4.27}$$

4.2.4 Magnetometer

The magnetometer measurements are very similar to the accelerometers. It measures a local magnetic field, $\mathbf{B}^N$, that is constant in the NED frame. The measurement equation is given by

$$\mathbf{y}^{mag} = C_b^n \mathbf{B}^N + \mathbf{e}^{mag} \tag{4.28}$$

where the measurement $\mathbf{y}^{mag}$ is the calibrated measurement. This model is only persistent under the assumption that $\mathbf{B}^N$ is constant, which is not the case if the aircraft is moving over large distances. In this case a GPS or accurate INS is required together with a model over the earth's magnetic field must be used to calculate $\mathbf{B}^N$.

4.2.5 Pitot tubes

From the pitot tube height and speed is calculated to be used as virtual measurements. The desired measurements are given by

$$\mathbf{y}^{pitot} = \begin{pmatrix} h \\ C_b^n v_a \end{pmatrix} \tag{4.29}$$

where h is the height over sea level and v_a is the air speed experienced in the body frame. Depending on what model is to be used the latter measurement must be adjusted. This is because when a vehicle is flying in side-winds its direction of velocity is not the same as the heading. If the difference between angle of velocity and heading is set to β the equation is adjusted to

$$\mathbf{y}^{pitot} = \begin{pmatrix} h \\ C_b^n v_a \cos(\beta) \end{pmatrix} \tag{4.30}$$

The virtual measurement for height, h, is the same here as in Section 4.1 according to

$$h = K \log\left(\frac{P_{s0}}{P_s}\right) + h_0. \tag{4.31}$$

The velocity is calculated using two pitot tubes, one that measures the static pressure, P_s, and one that measures the stagnation pressure, P_t. The second pitot tube is oriented in a desired direction where the velocity is to be calculated. If the density of the air is ρ, using Bernoulli's equation the velocity is given by

$$P_t = P_s \left(\frac{\rho v_a^2}{2}\right) \iff \tag{4.32}$$

$$v_a = \sqrt{\frac{2(P_t - P_s)}{\rho}} \tag{4.33}$$

As described here, all the parameters, P_{s0}, h_0 and ρ is estimated at start up of the vehicle. The parameter K is estimated in real-time as described in Section 4.1. A warning should be issued when using this model as well since the pressure reference at ground level may change over time.

4.2.6 GPS

The GPS measures the position in longitude and latitude. Since the positions are given in longitude and latitude in the filter the measurement equation is given by:

$$\mathbf{y}^{\mathbf{GPS}} = \mathbf{p} \tag{4.34}$$

4.3 Wind estimation model

This model is derived under the assumption that an Extended Kalman Filter is to be used together with measurements from GPS and pitot tube, [3]. Similar to equation (4.32) we can use Bernoulli's equation by assuming that the square of the airspeed is proportional to the dynamic pressure according to

$$v_{\text{pitot}}^2 = K\Delta P \tag{4.35}$$

where ΔP is the dynamic pressure as described in 3.4. If the vehicle is flying with an angle of attack or with side slip, the pitot tube will measure the airspeed, v_a, according to

$$v_{\text{pitot}} = |v_a|^2 \cos\alpha \cos\beta. \tag{4.36}$$

We can now solve for v_a^2,

$$v_a^2 = \frac{v_{\text{pitot}}^2}{\cos\alpha\cos\beta} = \frac{K\Delta P}{\cos\alpha\cos\beta} = \frac{\Delta P}{K_a}. \tag{4.37}$$

Here, K_a is a scale factor between dynamic pressure and the square of the airspeed. In flight it is not possible to interpret K_a as a constant since it depends side slip and attack angle. This factor must consequently be estimated during flight. We now propose the following state space model for use in wind estimation:

$$\begin{pmatrix} \dot{K_a} \\ \dot{v_w} \\ \dot{\phi_w} \end{pmatrix} = \begin{pmatrix} 0 & 0 & 0 \\ 0 & 0 & 0 \\ 0 & 0 & 0 \end{pmatrix} \begin{pmatrix} K_a \\ v_w \\ \phi_w \end{pmatrix} + \begin{pmatrix} 1 & 0 & 0 \\ 0 & 1 & 0 \\ 0 & 0 & 1 \end{pmatrix} \begin{pmatrix} v^{K_a} \\ v^{v_w} \\ v^{\phi_w} \end{pmatrix} \tag{4.38}$$

In the proposed model, v_w, is the wind strength and, ϕ_w, is the wind direction. The relation between the velocities can be seen in Figure 4.1.

4.3.1 Measurement equations

With the pitot tube we can measure the dynamic pressure,

$$y = \Delta P + v_p \tag{4.39}$$

$$v_p \sim N(0, R_p) \tag{4.40}$$

which we must relate to the wind model. From the wind triangle in Figure 4.1 we can, using Cosine's law, derive a relationship according to

$$v_g^2 + v_w^2 - 2v_g v_w \cos(\phi_w - \phi_g) = v_a^2. \tag{4.41}$$

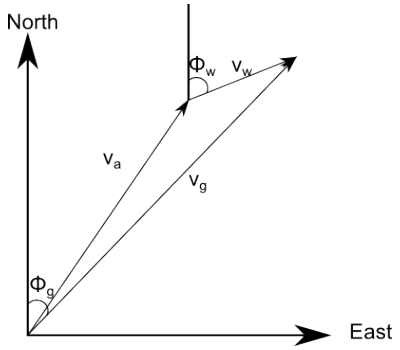

Figure 4.1. The different components contributing in a measurement v_a.

Under the assumption that the GPS velocity and heading are correct at every pitot measurement these can be interpreted as constants. From equation (4.37) and (4.41) we can now formulate

$$v_g^2 + v_w^2 - 2v_g v_w \cos(\phi_w - \phi_g) = \frac{\Delta P}{K_a} \iff \tag{4.42}$$

$$K_a \left(v_g^2 + v_w^2 - 2v_g v_w \cos(\phi_w - \phi_g)\right) = \Delta P. \tag{4.43}$$

The non linear measurement equation for estimating the wind is given by

$$y = K_a \left(v_g^2 + v_w^2 - 2v_g v_w \cos(\phi_w - \phi_g)\right) + v_p \tag{4.44}$$

4.4 Models with input signals

The models previously depicted has no input signals. Of course, a model for specific planes can be modified to hold inputs such as throttle, rudder and so on. How signals like these propagates through an arbitrary system is unknown and would have to be modelled for every specific aircraft.

However, measurements can be interpreted as input signals to a system. If a sensors measures the acceleration and speed according to,

$$\bar{\mathbf{y}} = \begin{pmatrix} \mathbf{a} \\ \mathbf{v} \end{pmatrix} \tag{4.45}$$

this can be translated into an input to the system,

$$\dot{\mathbf{p}} = \mathbf{v} \tag{4.46}$$

$$\dot{\mathbf{v}} = \mathbf{a}. \tag{4.47}$$

This approach can sometimes decrease complexity of the model since it might not be needed to include extra states to be able to include the measurements.

4.5 Linearization and discretization

Since the main focus of this thesis is to implement an real time extended Kalman filter all equations must be discretized and linearized. The discretization is achieved by euler forward method,

$$\dot{x} = \frac{x_{k+1} - x_k}{T_s} \tag{4.48}$$

where T_s is the sampling time. This is a simple approach but it is often sufficient. The linearization is done by taking the partial derivative of the states and measurement equations,

$$f(x) = \left.\frac{\partial f}{\partial x}\right|_{x=x_0} \cdot x = \left[\left.\frac{\partial f}{\partial x_1}\right|_{x=x_0}, \left.\frac{\partial f}{\partial x_2}\right|_{x=x_0}, \ldots, \left.\frac{\partial f}{\partial x_n}\right|_{x=x_0} \right] x \tag{4.49}$$

where x_0 is the linearization point. In practice when linearizing the states and measurement equation, x_0 is the last state estimation. This can yield problems when initializing the filter with the states x_0 and using the linearization around this point to update the filter, since the linearization around the correct state estimate could be completely different.

All the necessary linearizations of the states and measurement equations given in this chapter can be found in appendix A.

Chapter 5

Filtering

In this chapter different filter approaches that have been used are presented in their general form. The filters are then applied to the models described in Chapter 4 and the results are presented in Chapter 6.

5.1 Kalman filtering

The Kalman filter was derived 1960 in [13] and is derived using state space models according to,

$$x_{k+1} = F_k x_k + G_{u,k} u_k + G_{v,k} v_k \tag{5.1}$$
$$y_k = H_k x_k + D_k u_k + e_k \tag{5.2}$$
$$\tag{5.3}$$
$$Q_k = \mathrm{Cov}(v_k) \tag{5.4}$$
$$R_k = \mathrm{Cov}(e_k) \tag{5.5}$$

where x are the states and y are the measurements. A linear unbiased filter, see [9], is then given by

$$\hat{x}_{k+1} = F_k x_k + K_k(y_k - H_k x_k) \tag{5.6}$$

as long as $y_k - H_k x_k$ is a zero mean stochastic variable. The Kalman filter chooses the gain K_k, called the Kalman gain, optimal to minimize the covariance of

$$\tilde{x} = x - \hat{x}, \tag{5.7}$$

where x are the true states and $\hat{x}$ are the estimated states. A derivation of the Kalman filter can be seen in [9].

The fact that the Kalman filtering requires a system in state space form makes it applicable in many fields. It is also a filter that works well in real time if there is sufficient computational power.

5.1.1 Kalman filter

The ordinary Kalman filter requires linear system dynamics as given in (5.1). At every iteration in the filter there is a measurement update, which adjust the states according to measurements, and a time update that propagates the states according to the system dynamics. The standard Kalman filter is given in Algorithm 3, where the states, $\hat{x}$, and the error covariance, P_k are initialized by,

$$\hat{x}_{1|0} = \mathrm{E}(x_0) \tag{5.8}$$
$$P_{1|0} = \mathrm{Cov}(x_0) \tag{5.9}$$

Algorithm 3 The Kalman filter

1. **Measurement update:**

$$K_k = P_{k|k-1}H_k^T(H_kP_{k|k-1}H_k^T + R_k)^{-1}$$
$$\hat{x}_{k|k} = \hat{x}_{k|k-1} + K_k(y_k - H_k\hat{x}_{k|k-1} - D_ku_k)$$
$$P_{k|k} = P_{k|k-1} - K_kH_kP_{k|k-1}$$

2. **Time update:**

$$\hat{x}_{k+1|k} = F_k\hat{x}_{k|k}$$
$$P_{k+1|k} = F_kP_{k|k}F_k^T + G_{v,k}Q_kG_{v,k}^T$$

5.1.2 Extended Kalman filter

In many applications the state dynamics are non-linear,

$$x_{k+1} = f(x_k, u_k, v_k) \tag{5.10}$$
$$y_k = h(x_k, u_k, e_k). \tag{5.11}$$

In these cases the ordinary Kalman filter cannot be applied since the Kalman gain can not be calculated in a conventional way. The solution is to calculate the Jacobians of $f(x_k, u_k, v_k)$ and $h(x_k, u_k, v_k)$ and further assume that the noise is Gaussian,

$$x_{k+1} = f(x_k, u_k) + v_k \tag{5.12}$$
$$y_k = h(x_k, u_k) + e_k. \tag{5.13}$$

There is no guarantee that this is an optimal filter, it is not even guaranteed that it converges or is observable. If there are few non linearities this is often not a problem, but with system with lots of non-linearities these effects must be investigated carefully. The Extended Kalman filter is given in Algorithm 4.

It is worth to notice that all linear states in the extended Kalman filter is handled the same way as in the linear Kalman filter.

Algorithm 4 The Extended Kalman filter

1. **Linearize measurements:**

$$H_k = \left.\frac{\partial h(x,u)}{\partial x}\right|_{x=\hat{x}_{k|k-1}}$$

2. **Measurement update:**

$$K_k = P_{k|k-1}H_k^T(H_kP_{k|k-1}H_k^T + R_k)^{-1}$$
$$\hat{x}_{k|k} = \hat{x}_{k|k-1} + K_k(y_k - H_k\hat{x}_{k|k-1} - D_ku_k)$$
$$P_{k|k} = P_{k|k-1} - K_kH_kP_{k|k-1}$$

3. **Linearize dynamics**

$$F_k = \left.\frac{\partial f(x,u)}{\partial x}\right|_{x=\hat{x}_{k|k}}$$

2. **Time update:**

$$\hat{x}_{k+1|k} = f(\hat{x}_{k|k}, \hat{u_k})$$
$$P_{k+1|k} = F_kP_{k|k}F_k^T + G_{v,k}Q_kG_{v,k}^T$$

5.1.3 Iterated Kalman filter

One of the problems when implementing a Kalman filters in real time systems is to calculate the inverse,

$$(H_kP_{k|k-1}H_k^T + R_k)^{-1}. \tag{5.14}$$

The dimension of the matrix inversion is the same as the number of measurements.

Micro controllers used in real time applications are optimized for energy consumption and low cost. As a consequence they have lower clock frequency than commercial processing units. When implementing a filter on a micro controller, primitive programming languages such as C is often used. This means that there is a need for fast inversion routines for solving large matrix inversions in real time.

In an iterated Kalman filter, there are two or more sequential measurement updates, thus decreasing the dimension of the matrix inversion. Measurement updates can be done sequentially if the measurements are independent. A derivation and an intuitive proof is given in [8].

If all sensor measurements are independent the matrix inverse can be avoided all together. This form of the Kalman filter yields great advantages when implementing a Kalman filter on a micro controller. Indirectly, this also gives the opportunity to handle information from sensors that delivers data in different frequency. When information from a sensor becomes available, the filter is updated

with all available information followed by a time update step. The iterated Kalman filter is given in Algorithm 5.

Algorithm 5 The iterated Kalman filter

1. **Measurement update:**

   For i = 1,2,...,M,

   $$K_k^i = P_{k|k-1}^{i-1}(H_k^i)^T(H_k^i P_{k|k-1}^{i-1}(H_k^i)^T + R_k^{ii})^{-1}$$
   $$\hat{x}_{k|k}^i = \hat{x}_k^{i-1} + K_k^i(y_k^i - H_k^i\hat{x}_k^{i-1} - D_k u_k)$$
   $$P_{k|k}^i = P_{k|k-1}^{i-1} - K_k^i H_k^i P_{k|k-1}^{i-1}$$

   Then,

   $$\hat{x}_{k|k} = x_k^M$$
   $$P_{k|k} = P_k^M$$

2. **Time update:**

   $$\hat{x}_{k+1|k} = F_k\hat{x}_{k|k}$$
   $$P_{k+1|k} = F_k P_{k|k} F_k^T + G_{v,k}Q_k G_{v,k}^T$$

The algorithm for the iterated Kalman filter can be adjusted to work as an iterated extended Kalman filter. This is done by adding the linearization steps from algorithm 4 to the algorithm for the iterated Kalman filter.

5.2 Recursive Least Squares

The Recursive Least Squares is an adaptive filter [9] that minimizes the criteria

$$\hat{\theta}^{\mathrm{RLS}}(t) = \arg\min_{\theta} V_t(\theta) \tag{5.15}$$

$$V_t(\theta) = \sum_{k=1}^{t} \lambda^{t-k}\left(y(k) - \phi^T(k)\theta\right)^2 \tag{5.16}$$

where λ is a forgetting factor that decreases exponentially in time. The forgetting factor will make sure that old measurements does not affect the parameter estimation as much as newer measurements. λ is constrained to $[0, 1[$ and typical values are between 0.9...0.999. The RLS algorithm can be used to estimate parameters in a model that changes over time. If a parameter has a tendency to change much over time, λ should be around 0.95, and if it is constant over time, λ should be close to 1.

Algorithm 6 Recursive Least Squares(RLS)

For a linear regression model, $y(t) = \phi^T(t)\theta(t) + e(t)$ The RLS algorithm for parameter estimation is given by:

$$\hat{\theta}_k = \hat{\theta}_{k-1} + K_k(y_k - \phi_k^T \hat{\theta}_{k-1})$$
$$K_k = \frac{P_{k-1}\phi_k}{\lambda + \phi_k^T P_{k-1}\phi_k}$$
$$P_k = \frac{1}{\lambda}\left(P_{k-1} - \frac{P_{k-1}\phi_k\phi_k^T P_{k-1}}{\lambda + \phi_k^T P_{k-1}\phi_k}\right)$$

λ is a design parameter that decides how much old measurements will be weighted in to the estimation.

Algorithm 6 describes the algorithm for the Recursive Least Squares and is given in [9].

Chapter 6

Results

The main focus was to use an Iterated EKF, as described in Section 5.1.3, with the 22 state model, Model 1, as presented in Section 4.2, the wind estimation and the height estimation. The EKF never became fully functional during this thesis and therefore the other models were not evaluated. Probable causes to why it did not work are presented and suggestions on how to get it running are proposed.

6.1 Perturbed magnetic fields

To be able to evaluate the filter, data from flights were needed. The initial flights showed that the magnetometer and accelerometer could not be fused. After calibration, the magnetometer and accelerometer were aligned, but when in flight they were not.

The source of this problem was magnetic fields, generated by the cables powering the motor. In this section, the source of the problem is explained and a solution is proposed.

6.1.1 Electrical disturbances

When a high current runs through a wire a magnetic field will be induced as illustrated in Figure 6.1. At each point in the room, the magnetic fields are additive. This will create problems with the magnetometer reading since the only magnetic field that is of interest, is the earth's magnetic field. If the exact magnitude of the magnetic fields created by wires are unknown there is no way to know the earth's magnetic contribution in a given point. A less obvious problem is caused by induced currents. If $\bar{B}$ is the magnetic field, $\bar{H}$ is the magnetizing field, $\bar{J}$ is the net electrical current and $\bar{M}$ is the magnetization, Maxwell's equation states that

$$\nabla \times \bar{H} = \bar{J} + \frac{\partial \bar{D}}{\partial t} \tag{6.1}$$

$$\bar{B} = \mu_0 \left(\bar{H} + \bar{M} \right). \tag{6.2}$$

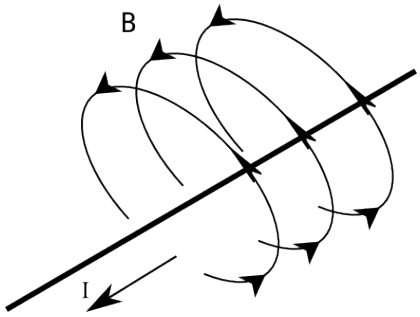

Figure 6.1. A current, I, runs through a wire and creates the magnetic field B.

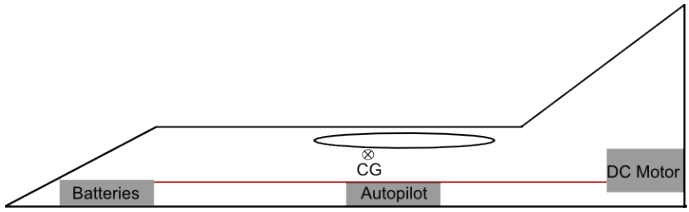

Figure 6.2. A common layout to achieve a center of gravity under the wings when constructing small planes.

For a detailed description of these equations, see [6]. What is of interest here is that a current, $\bar{J}$, will be induced if the magnetic field, $\bar{B}$ is time varying. Ideally, a direct current will not be time varying, but this is not the case when there is a lot of electronics and a motor connected to the power source.

6.1.2 Small airframes

These kinds of problems can be avoided, simply by not mounting the sensors close to high current wires. But when building planes, the components can not be mounted arbitrarily. This is particularly the case for small airframes with rear mounted engines. This kind of planes can not take a lot of payload, the weight must be kept at a minimum. But for the plane to be able to fly well, the center of gravity should be located at a correct position under the wings. The two main components that decide where the center of gravity will be is the motor and the batteries. These are the two heaviest components in the plane, and since the motor is rear mounted the batteries must be mounted in the front of the plane, see Figure 6.2.

With this construction, the wires powering the DC motor will run parallel with the autopilot. Since the motor draws more than 30 amperes this can cause problems for the autopilot.

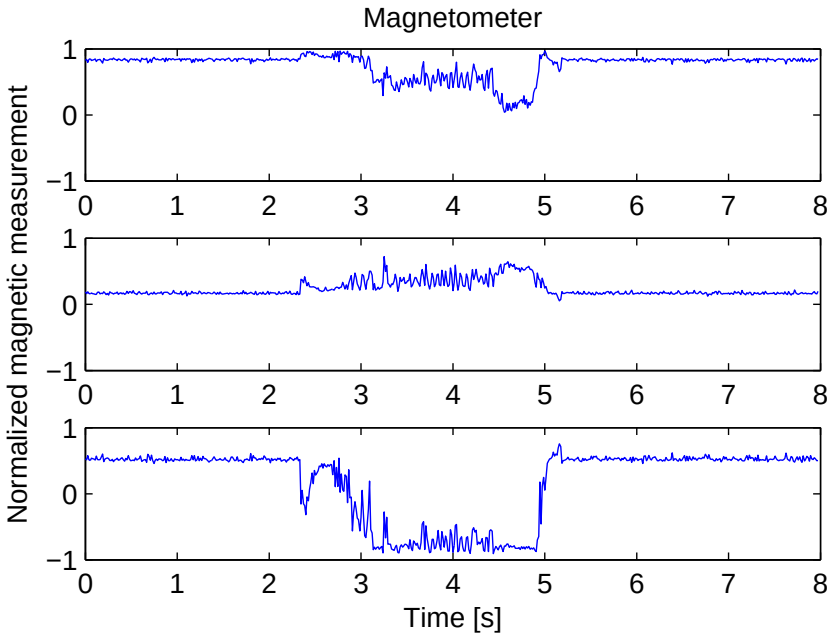

Figure 6.3. Normalized magnetometer measurements when aircraft is at stand-still with normal wiring. After two seconds the engine is started.

6.1.3 Disturbance analysis

The effect of disturbances caused by the induced fields by the wires is analyzed by fixating the plane to the ground. The autopilot is mounted parallel to the wires powering the DC motor. In Figure 6.3 it is obvious that the magnetic field becomes severely distorted when the motor starts after 2 seconds. The distortion will be proportional to the current feeding the DC motor, so this is not a constant field that can be compensated for in a simple way.

When the motor starts the magnetometer's z-axis changes from a huge positive number to a huge negative number. In Sweden, the downward component of the earth's magnetic field is the largest one. If it switches sign the magnetometer will indicate that the autopilot is upside down, so it is clear that these readings are useless whilst the motor is running. As discussed, the magnetic field created by the electrical current affected the magnetometer reading a lot, we can also see that the noise level increases. That induced currents affects other MEMS sensors as well, which can be seen in Figure 6.4. When the motor starts after 2 seconds the noise level increases dramatically on the accelerometer, and this goes for all the sensors. The difference between the accelerometer and the magnetometer is that a bias is not introduced, just an increase of noise. This can be understood from (6.1). The induced currents is caused by fluctuations in the magnetic field. Since the current is not held constant in wires delivering power to the DC motor the magnetic field will not be constant either. When the magnetic field temporarily increases it

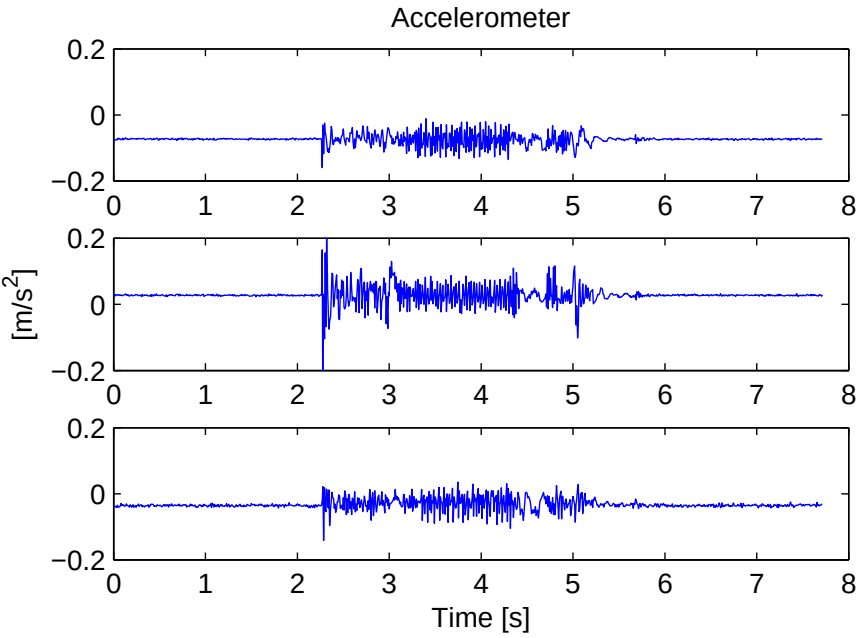

Figure 6.4. Accelerometer measurements when aircraft is at stand-still with normal wiring. After two seconds the engine is started.

will introduce currents in one direction, when the magnetic field decreases it will introduce currents in the opposite direction. The output of the MEMS sensors are analog and converted to digital values by an A/D converter. These fluctuations in induced currents will cause temporary misreads by the A/D converter, and this is the cause of the increased noise of the MEMS sensors. In Figure 6.5 the part of the accelerometer measurement where the motor is running is cut out and plotted in the frequency domain. This gives information about the fluctuation in the magnetic field caused by the wires in the fuselage. If a relationship between the speed of the motor and the induced fluctuations can be described the noise problems can probably be solved by a notch filter. But even if this is successful, the problem with the magnetometer will still exist.

6.1.4 Minimizing electrical disturbances

If possible, the cables powering the motor should not be placed parallel with the autopilot, if the construction of the aircraft allows this. With small aircraft this might not be an option. The most obvious way to solve the problem is to use shielded cables.

A very simple way of reducing the noise is to twist the wire that delivers current to the motor with the wire that connects back to the ground and to shield the cable with a metal foil or with a metal braiding and connect it to ground. This will divert the magnetic field to a path through the foil or braiding so that the

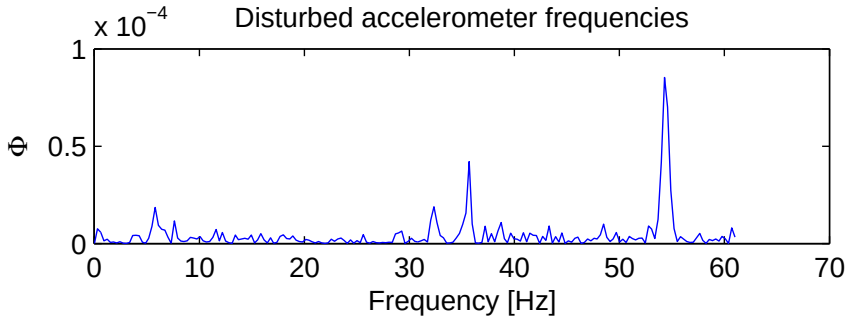

Figure 6.5. Frequency analysis of the electrically disturbed accelerometer.

disturbing magnetic field does not affect the autopilot. In an aircraft there is no true ground, and therefore the battery's ground should be used.

The cable constructed for these experiments consists of a braided and twisted cable. The metal braiding is connected to the ground. The same experiment as described in 6.1.3 is performed. How well the disturbing magnetic fields are suppressed can be seen in Figure 6.6. The motor starts after 2 seconds, but there is no indications of external magnetic fields. The accelerometer measurements can be seen in Figure 6.7, and there is no longer an increase in noise levels when the motor starts.

From Section 6.1.3 we can see how important it is to minimize the electrical disturbances that can be caused by improper wiring. A very simple, but very effective, way of improving the measurements that requires no special cables are proposed and should always be done if no shielded power cables to the motor are available.

6.2 GPS issues

When introducing movement to the system, the accelerometer could not be fused with the GPS. During the thesis, it became clear that an arbitrary GPS cannot be used. In this section, experienced problems with the GPS are explained and a solution is proposed.

6.2.1 GPS Modes

A GNSS is desirable to have in many different types of systems, from hand-held devices to high speed aircraft. These two examples have very different requirements on the GNSS. For example, the pedestrian is not interested in momentary changes in position in velocity but wants to have a smooth position estimate with low noise. The aircraft on the other hand moves very fast and needs to know the momentary position. The manufacturers of GNSS chips often provides some kind of filtering in their modules. A typical hand-held device may have one second delay position

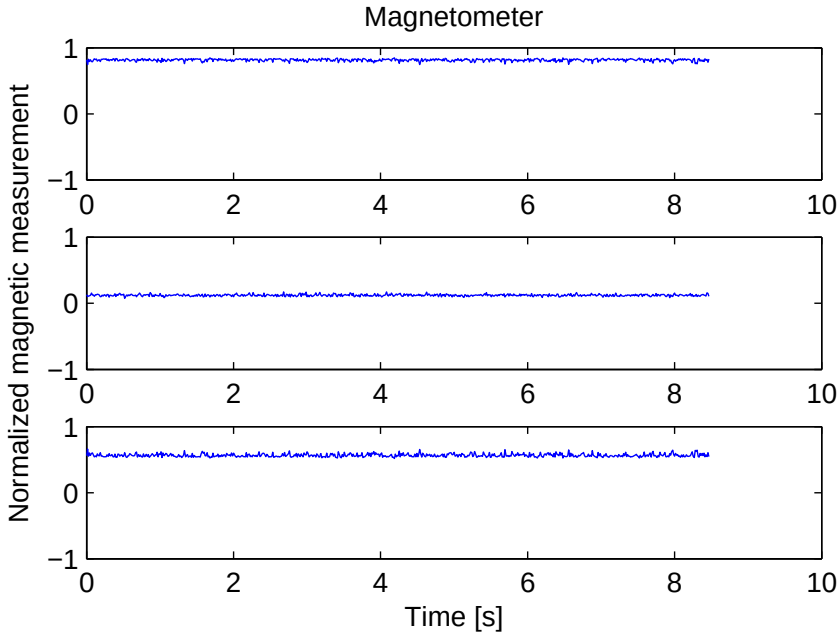

Figure 6.6. Normalized magnetometer measurements when aircraft is at stand-still with shielded wiring. After two seconds the motor is started.

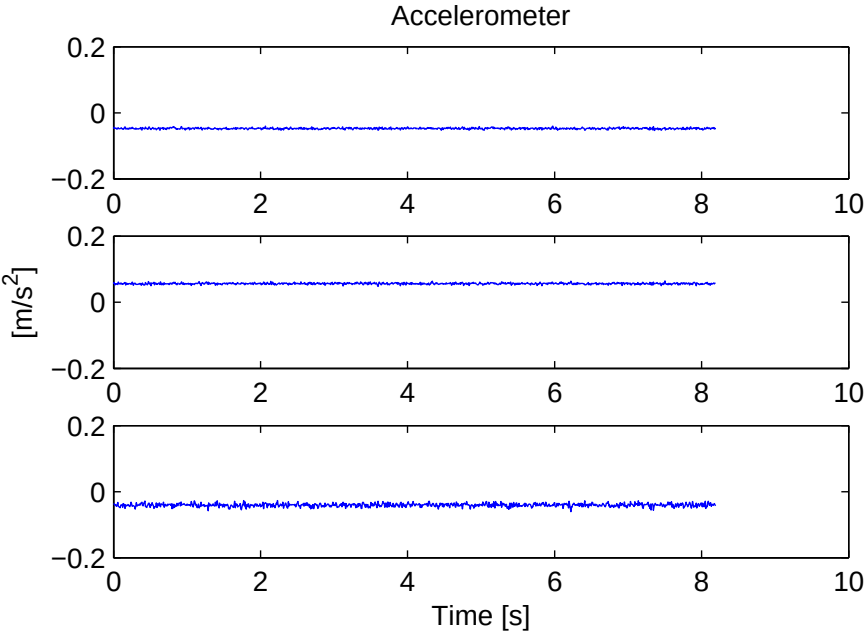

Figure 6.7. Accelerometer measurements when aircraft is at stand-still with shielded wiring. After two seconds the motor is started.

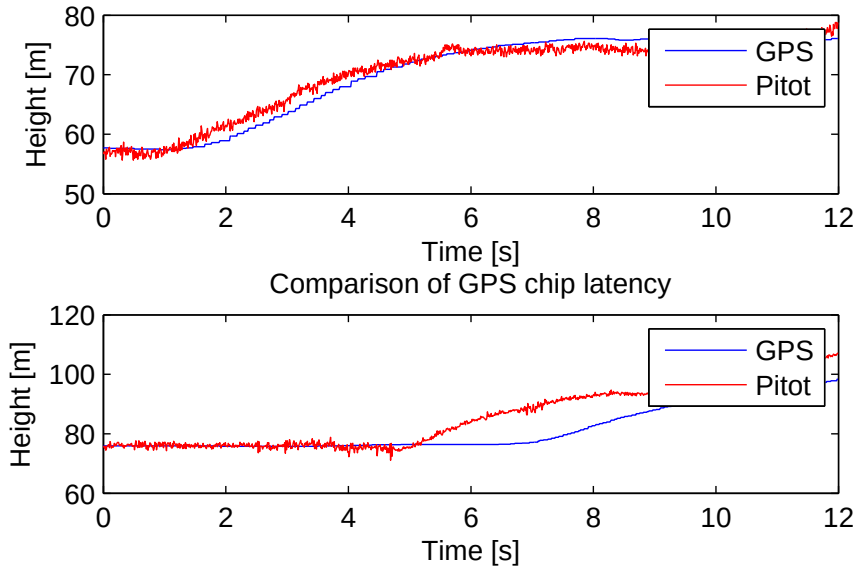

Figure 6.8. Two GPS chips measuring height compared to height derived from static pressure measured by a pitot tube. The lower is a GPS set in pedestrian mode.

and velocity measurements due to extensive filtering. In this case this is desired because the pedestrian moves slowly in small areas, and one second delay in the measurements does not matter. On an aircraft moving in over $100m/s$ this can be devastating, especially in real time systems, since it will always acquire a position estimate that is $100m$ off. If internal filtering is turned off, noise on the position and speed estimate will increase but the measurement will be up to date. In Figure 6.8 two different GPS chips are used. The height from the GPS chips is compared to the height indicated by a static pressure sensor.

Unfortunately, the latency is not always provided by the manufacturer, nor is it guaranteed.

6.2.2 Variable latency

Even though the mode of the GPS is important, this is something that can be evaluated by studying data sheets and second hand information. A problem that was discovered with the GPS used on the EasyPilot was variable latency. This was hard to prove from collected data since the main accelerations in an airframe is during coordinated turns. It is difficult to generate plots that makes sense from a rotating accelerometer and a variable latency GPS.

The manufacturer of the chip provided information and plots that concluded that there was variable latency on the GPS. These can however not be published due to confidentiality.

6.2.3 GPS conclusions

The choice of GPS is not trivial, especially when GPS data is to be fused with other sensors. The GPS used on EasyPilot was considered not fit for high acceleration turning vehicles. With this said, it is probably not a bad GPS, it is only applied to the wrong application.

For sensor fusion, low latency and little filtering is desired. If a GPS module is using extensive filtering, it will probably suffer in latency and the noise on the output is unknown.

The solution to the GPS problems is to replace it. A new GPS suitable for high acceleration applications should be used for EasyPilot to improve the abilities to fuse sensor data in a proper manner.

6.3 22 state EKF

In this section, the results of the 22 state EKF are presented.

6.3.1 Position and Velocity estimation

The position and velocity estimation did not work when adding GPS to the measurement equations of the EKF. It is difficult to know for sure why this is the case. When the GPS is added, the accelerometer bias states is estimated incorrectly and the acceleration states will start to fluctuate. This has a great impact on gyroscope bias and estimated orientation. From this point it is hard to interpret what actually went wrong since all states seems to be estimated incorrectly.

There are four probable causes to this problem, or a combination of the three:

GPS latency: As described in Section 6.2, there was a very significant latency from the GPS used on the autopilot. This means that the accelerometer and GPS will feed the filter with contradictory information during acceleration and deceleration.

GPS filtering: The GPS also had a very strange filter providing position estimates. It could be smooth for a while and then jump to another value. The inconsistency on the GPS estimates could cause strange behavior in the filter.

Magnetic field disturbances: If there are magnetic field disturbances, the magnetometer and accelerometer will feed the filter with contradictory information, thus causing the acceleration bias to be estimated incorrectly.

Improper tuning: The filter might be tuned incorrectly. It is a difficult task to tune an EKF, especially when the cause of the problems are unknown.

During this master thesis, the conclusion that a combination of GPS latency and internal GPS filtering is the probable cause has been taken. This is because it has been shown that the GPS has significant errors and because the filter is working properly as long as there are no motions present.

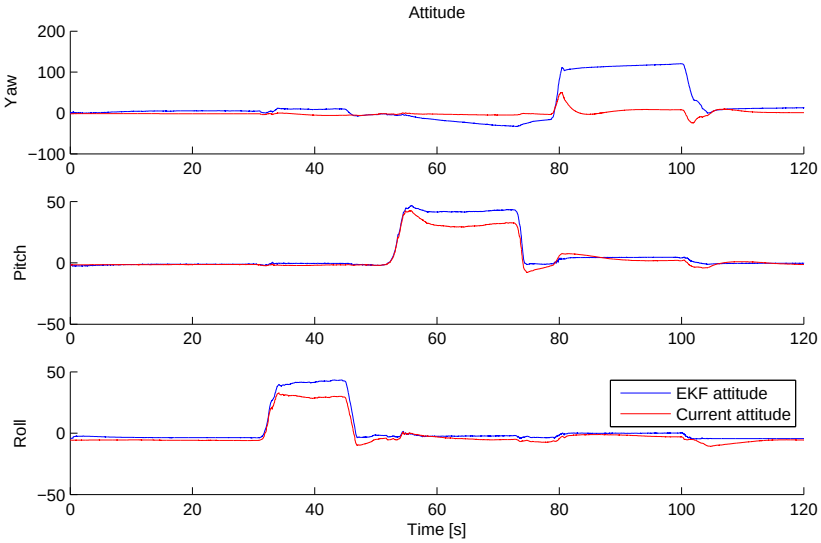

Figure 6.9. Estimated attitude by the EKF compared with the current attitude estimation on the autopilot.

6.3.2 Attitude estimation

Since no external references of the attitude are present, the tests are done in a controlled environment. First, the autopilot is laying flat and still so that references for gyro biases can be calculated. Then the following motions are performed:

Roll - Roll to 45°, then roll back to original position.

Pitch - Pitch to 45°, then pitch back to original position.

Yaw - Yaw 120° from original position, then yaw back to original position.

In Figure 6.9 the estimated attitude is presented. There is a good result in pitch and roll, but the yaw angle is converging slowly after the gyroscopes has updated the states. This is because there is very little information about the yaw angle from the available measurements. The earth's magnetic field has very high inclination in Sweden and the gravity is always pointing to the center of the earth. Because of this there is very little information in yaw angle. After the gyroscopes has updated the quaternions the yaw angle reaches approximately 110°, then it takes almost 20 seconds for the quaternions to converge.

This calls for careful calibration of the gyroscopes scaling factors. If the gyroscopes are well calibrated, the other sensors would only need to stabilize the estimates whilst the gyroscopes takes care of the quaternion propagation.

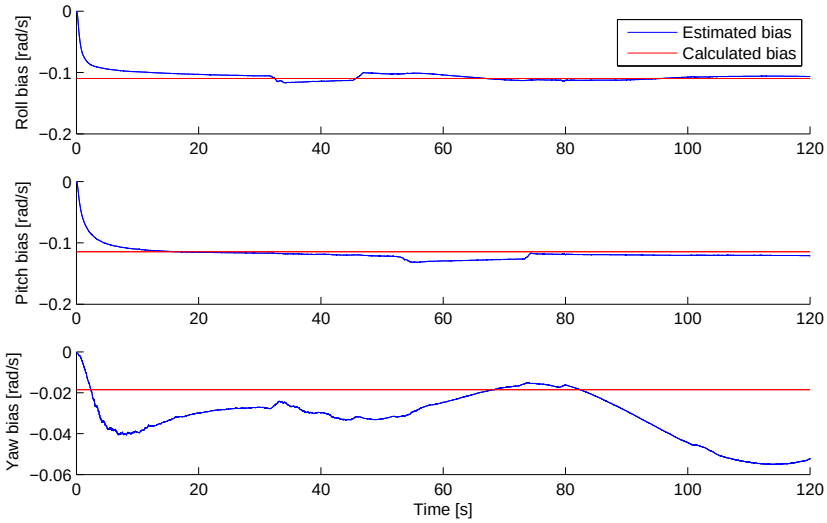

Figure 6.10. Gyroscope biases estimated by the EKF compared with biases calculated from mean.

6.3.3 Bias estimation

In Figure 6.10 the gyroscope biases are presented. These are of great importance if the gyroscopes are to be used for propagation of the quaternions. The red line is the calculated mean of the gyroscope measurements when the autopilot is at stand-still. The same discussion as for the attitude angles holds for this results to, there is little information from other sensors of the yaw-motion when oriented horizontal. The bias in roll and pitch angle works fine since the magnetometer and accelerometer measurements does not change.

The accelerometer bias is harder estimate and also to evaluate. The true bias of the accelerometer is unknown, since the accelerometer output is based on orientation. To calculate true biases the exact position of the accelerometer chip must be known. Unfortunately the accelerometer chip orientation is not known, so the error caused by orientation uncertainties would probably be larger than the bias.

The bias estimated by the filter can be seen in Figure 6.11. Here we can see that the bias seems to converge to different values depending on orientation. One sensor that is used to estimate the bias in the Extended Kalman filter is the magnetometer. If the magnetometer and accelerometer is misaligned they will deliver contradictory information about orientation. This conflict is resolved by the Extended Kalman filter by changing the accelerometer biases. The conclusion from Figure 6.11 is that a sensor misalignment calibration might be necessary.

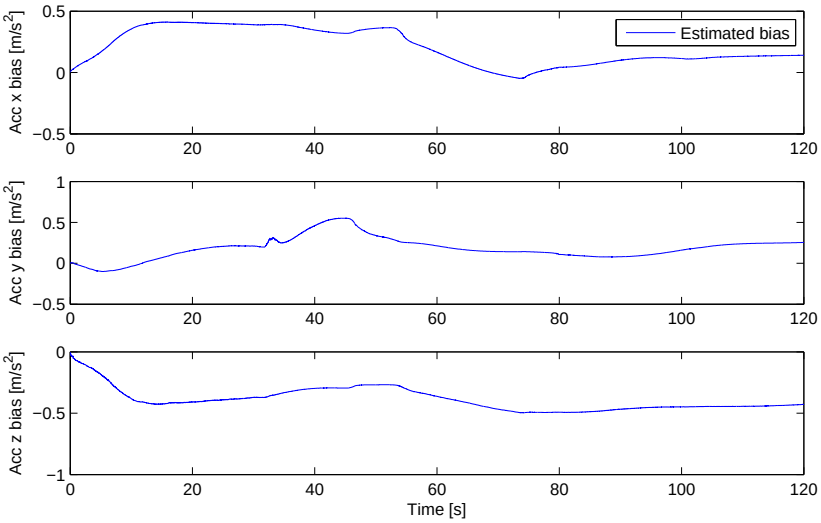

Figure 6.11. Accelerometer biases estimated by the EKF.

6.4 EKF wind estimation

The Extended Kalman Filter for wind estimation is based on the models derived in 4.3. The test was performed with the autopilot flying the aircraft in a square at fixed altitude. In Figure 6.12 we can see the GPS speed and the airspeed measured during the flight. The autopilot always flies by airspeed, and in this flight the airspeed reference was set to 20 $[m/s]$. The weather information from the day of the flight indicated a wind at 5 $[m/s]$.

From Figure 6.12 we can estimate the wind speed and direction by studying the relationship between airspeed and ground speed. When the ground speed is higher than the indicated airspeed we are flying with tailwind and when the ground speed is lower we have a headwind. By measuring the distance between the valleys and the peaks in the ground speed we can get a rough estimate of the speed of the wind according to

$$v_w = \frac{v_g^{\max} - v_g^{\min}}{2}. \tag{6.3}$$

From the plots in Figure 6.12 we can get an indication that the wind speed is somewhere between 5 and 7 $[m/s]$. We can also look at interval where the ground speed has it's minimum and compare this with the heading. From the plots we can see that the aircraft has it's strongest headwind whilst heading $290 - 300°$. This indicates that we have a north-northwest wind at $5 - 7$ $[m/s]$.

In Figure 6.13 the result of the Extended Kalman filter is illustrated. The wind speed is estimated to around -6 $[m/s]$ and the heading of the wind is estimated to

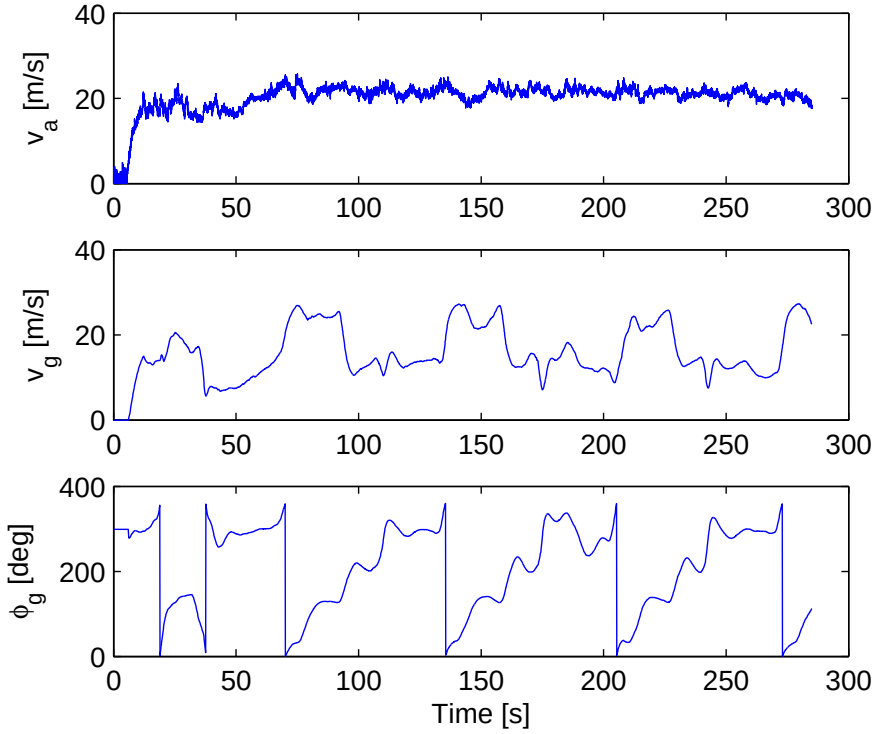

Figure 6.12. Measured wind speed, ground speed from GPS and heading from GPS

around $-65°$. Since north is defined as $0°$ we can add 360 degrees to our estimate, which gives an estimate of $295°$. When deriving the wind model we represent the wind as an angle and a speed, see Figure 4.1. This means that a negative wind speed at $295°$ is a positive wind speed in nort-northwest and this is what we would expect from the flight pattern given in Figure 6.12.

The estimated state, K_a, was defined as a function of the slip angle and angle of attack. Since this parameter fluctuates a lot the plane must have been flying with side slip or with an angle of attack. This induces uncertainties in the reasoning about wind speed and wind direction from Figure 6.12 since we can not be sure in which direction the plane is actually heading.

6.5 RLS parameter estimation

The RLS parameter estimation is used to estimate the constant, K, from (4.11). The estimation of this parameter is of importance if the GPS and static pressure sensor are to present the same altitude. In Figure 6.14 the GPS height, altitude

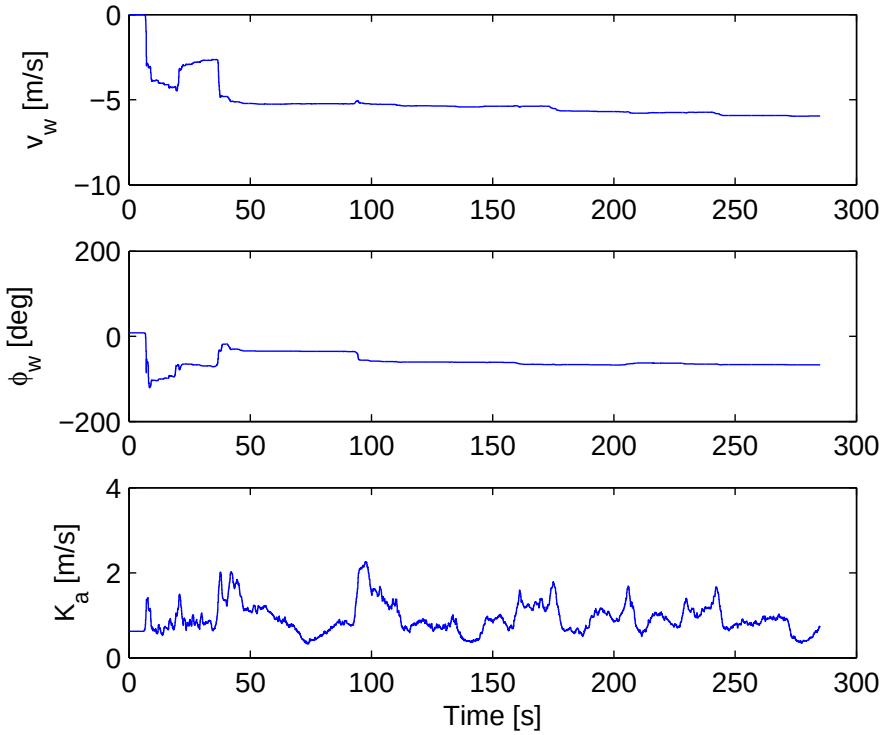

Figure 6.13. Estimated parameters for the wind model. v_w is the wind speed and ϕ_w the wind direction.

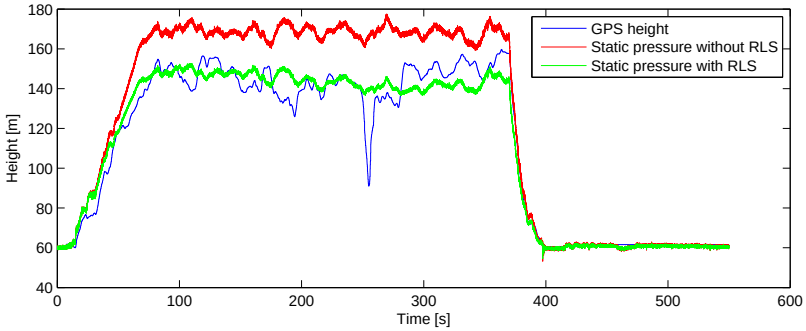

Figure 6.14. GPS height compared to height calculated from static pressure.

from the pressure sensor when K is constant and height from pressure sensor when K is estimated with RLS in flight. As seen in the Figure, the GPS height varies a lot. In this measurement series, the curvature from the pressure sensor is seen as the more reliable of the two. Even though the form of the curvature is correct, it is clear that a constant offset is persistent when flying at cruising altitude. The GPS does not have this weakness, even if the measurements fluctuates, it will not have an offset. It is this characteristic from the GPS height that can be utilized to improve the pressure measurement together with a RLS.

The updates should however be performed with care. After approximately 250 seconds in flight, the GPS measurement becomes erroneous, dropping almost 60 meters in a few seconds. If we follow the RLS adjusted height measurement, we can see that after this moment the mean value becomes lower than the GPS height. This error has apparently affected the parameter estimation a lot and it takes time for the parameter to converge to a correct value again. To avoid this problem, the RLS should not be invoked when the GPS height is considered unreliable.

Chapter 7

Conclusions and future work

7.1 Conclusions

In this master thesis the goal was to design and evaluate an Extended Kalman Filter for state estimation of an UAV. Complementary filters for wind estimation and for height measurement improvements have been presented as well. The filters have been implemented in Matlab, C# and C.

A large focus was put into the analysis of the magnetometer since it was considered to be of importance in the Extended Kalman filter. It is a very good sensor to have if it is working, but if it is not it will cause problems in the state estimation. Unfortunately, it is also very sensitive to disturbances which means it may become unreliable in an improper environment.

During the master thesis all work has been done using an existing autopilot with the sensors mounted. This have caused restriction of the work in some aspects, no sensors could be exchanged and they had to be sampled through the existing AHRS. This meant that software for logging and an extension of the autopilots communication protocol had to be developed. With this configuration, the highest delivery rate of sensor data was limited to 122Hz.

At a late stage of the master thesis data logging was done from actual flights. Around the mounting position of the autopilot there was major electrical and magnetic disturbances. These problems have also been discussed and solved in this master thesis.

Another issue that affects the possibilities to design this kind of Extended Kalman filter is the GPS. When developing a filter of this type, an arbitrary GPS chip will not do. A GPS chip may have all kinds of internal filtering and latencies. The GPS chip mounted on the used autopilot has increased latency when accelerating or decelerating, which means that the GPS and accelerometer will feed the filter with contradictory information during short periods of time. Another GPS that have been used had a constant latency at over 1s, thus yielding it useless.

During the beginning of the master thesis, when the sensors was evaluated and calibration algorithms were derived, a calibration for sensor misalignment should

have been derived as well. It is hard to confirm that there is a small misalignment on the mounted sensors, but indications that this might be the case exists.

The attitude estimation of the Extended Kalman filter is not superior to the current filter implemented in the AHRS. But the Extended Kalman Filter also estimates other states that is of interest in a controlled manner and eliminates the need for manual calibration of biases. Although the Extended Kalman filter that has been designed during this master thesis has a lot of benefits, in the state in which it is right now, it cannot compete with the robustness of the current AHRS. The steps required to make the Extended Kalman filter more robust consists of filter tuning, misalignment calibration, better GPS firmware and measurements should be audited if they are suitable for updating the filter.

7.2 Future work

Today, micro controllers are becoming increasingly faster together with float precision. This creates opportunities for implementing advanced filtering in real time system. Extended Kalman filters with complex state space models can now be updated by many measurement equations in a satisfying frequency. The proposed Extended Kalman filter holds great potential for small UAVs since it is shown that it is possible to use the filter with commercially available MEMS sensors and power efficient MCU's. Future work should be focused on the robustness of the Extended Kalman filter.

Another very interesting competitor to the Extended Kalman filter is the Unscented Kalman filter. This is a filter that handles the non-linearity problem in a better way than the Extended Kalman filter. Instead of calculating the Jacobians, the Unscented Kalman filter utilizes the Unscented transform to calculate sigma points. These are then propagated through the non-linearities. Since there are non-linearities in the quaternions the UKF may perform better than the EKF in this case.

Bibliography

[1] Cenk Acar and Andrei Shkel. *MEMS Vibratory Gyroscopes: Structural Approaches to Improve Robustness*.

[2] David W. Allan. Statistics of atomic frequency standards. *Proceedings of the Ieee*, 54(2), 1966.

[3] Cho Am, Kim Jihoon, Lee Sanhyo, and Changdon Kee. Wind estimation and airspeed calibration using the uav with a single-antenna gnss receiver and airspeed sensor. Technical report, School of Mechanical and Aerospace Engineering, Seoul National University, Korea, 2006.

[4] Frank J. Centinello III. Analysis of the ned and ecef covariance propagation for the navigational extended kalman filter. *International Astronautigal Congress*, 58, 2007.

[5] Tom Chalko. High accuracy speed measurement using gps (global positioning system). *Nujournal*, 2007.

[6] K David Cheng. *Field and Wave Electromagnetics*.

[7] Mark Euston, Paul Coote, Robert Mahoney, Jonghyuk Kim, and Tarek Hamel. A complementary filter for attitude estimation of a fixed-wing uav. Technical report, Automation and Robotics Laboratory - Aveiro University.

[8] Fredrik Gustafsson. *Statistical Sensor Fusion*. 1 edition, 2010. ISBN13: 978-91-44-05489-6.

[9] Fredrik Gustafsson, Lennart Ljung, and Mille Millnert. *Signal Processing*. 1 edition, 2010. ISBN13: 978-91-44-05835-1.

[10] Willem J. Hough. Autonomous aerobatic flight of a fixed wing unmanned aerial vehicle. Master's thesis, Stellenbosch University, 3 2007.

[11] I.Markovsky, A.Kukush, and S.Van Huffel. Consistent least squares fitting of ellipsoids. *Numerische Mathematik*, 98:177–194, 2004.

[12] Fredrik Johansson and Hugo Kinner. Sensorfusion för reglering av obemannad helikopter. Master's thesis, Linköping University, 2011.

[13] Rudolf E. Kalman. A new approach to linear filtering and prediction problems. *Journal of Basic Engineering*, 82(Series D), 1960.

[14] J L Marins, E R Bachmann, R B McGhee, and M J Zyda. An extended kalman filter for quaternion-based orientation estimation using marg sensors. *Proceedings 2001 IEEERSJ International Conference on Intelligent Robots and Systems Expanding the Societal Role of Robotics in the the Next Millennium Cat No01CH37180*, 4(2):2003–2011, 2003.

[15] Joao L. Marins. An extended kalman filter for quaternion-based attitude estimation. Master's thesis, United States Navy - Naval Postgraduate School, 9 2000.

[16] Valérie Renaudin, Muhammad Haris Afzal, and Gérard Lachapelle. Complete triaxis magnetometer calibration in the magnetic domain. *Journal of sensors*, 2010, 10 2010. ID 967245.

[17] Sven Rönnback. Development of a ins/gps navigation loop for an uav. Master's thesis, LuleåTekniska Universitet, 2 2000.

[18] Inc. SiRF Technology. *NMEA Reference Manual*. SiRF Technology, Inc., 2.1 edition, February 2007. Part Number: 1050-0042.

[19] Sensors Spectrum and Controls Inc. Compensating for accelerometer misalignments. Tech Note 413.

[20] Sherryl H. Stovall. Basic inertial navigation. Technical report, Navigation and Data Link Sectionm, Systems Integration Branch, 1997. http://www.fas.org/spp/military/program/nav/basicnav.pdf.

[21] David Titterton and John Weston. *Strapdown Inertial Navigation Technology*. The Institution of Electrical Engineers, 2 edition, 2004.

[22] David Törnqvist. *Estimation and Detection with Applications to Navigation*. PhD thesis.

[23] David Törnqvist. Statistical fault detection with applications to imu disturbances.

[24] u-blox ag, http://www.u-blox.ch. *Datum Transformation of GPS Position*, 7 1999.

[25] Martin Vagner. Mems gyroscope performance comparison using allan variance method. Technical report, FEEC BUT.

[26] Clas Veiback. Automatic control of unmanned aerial vehicles. Master's thesis, Uppsala University, 2010.

[27] Jean-Marie Zogg. Gps, essentials of satellite navigation. Technical Report GPS-X-02007-D, U-blox AG, 2009.

Appendix A

Linearization

When linearizing model and measurement equation the partial derivative is taken with respect to all states. The state space used to describe the linearizations here are *Model 2* as depicted in Section 4.2 with 24 states,

$$\mathbf{x} = \begin{pmatrix} \mathbf{p} \\ \mathbf{v} \\ \mathbf{a} \\ \mathbf{q} \\ \boldsymbol{\omega} \\ \mathbf{b}^a \\ \mathbf{b}^\omega \\ \mathbf{w} \end{pmatrix} \tag{A.1}$$

The point of linearization will be denoter x_0 throughout this appendix. Only the non zero parts of the linearization are presented.

Model linearization

The non linear parts of the model consists of $\dot{\mathbf{p}} = P(\mathbf{p})\mathbf{v}$ and $\dot{\mathbf{q}} = S(\boldsymbol{\omega})\mathbf{q}$. All other states in the presented models are linear.

Position propagation

The position propagation is given by

$$\dot{\mathbf{p}} = \mathbf{P}(\mathbf{p}) \cdot \mathbf{v}. \tag{A.2}$$

In matrix form this is

$$\begin{pmatrix} \dot{\lambda} \\ \dot{\phi} \\ \dot{h} \end{pmatrix} = \begin{pmatrix} 0 & \frac{1}{(a+h)\cos\phi} & 0 \\ \frac{1}{a+h} & 0 & 0 \\ 0 & 0 & h \end{pmatrix}. \tag{A.3}$$

The partial derivative with respect to $\mathbf{p}$ and $\mathbf{v}$ is then given by

$$\begin{pmatrix} \dot{\lambda} \\ \dot{\phi} \\ \dot{h} \end{pmatrix} = \tag{A.4}$$

$$\begin{pmatrix} 0 & \frac{V_E \sin\phi}{((a+h)\cos\phi)^2} & \frac{-V_E\cos\phi}{((a+h)\cos\phi)^2} & 0 & \frac{1}{(a+h)\cos\phi} & 0 \\ 0 & 0 & \frac{-V_N}{(a+h)^2} & \frac{1}{a+h} & 0 & 0 \\ 0 & 0 & 0 & 0 & 0 & -1 \end{pmatrix} \Bigg|_{x=x_0} \begin{pmatrix} \lambda \\ \phi \\ h \\ V_N \\ V_E \\ V_D \end{pmatrix} \tag{A.5}$$

$$= \begin{bmatrix} H_p & H_v & 0_{3\times 18} \end{bmatrix} \mathbf{x} \tag{A.6}$$

Quaternion propagation

The quaternion propagation is given by equation (2.50),

$$\dot{\mathbf{q}} = \frac{1}{2} S(\boldsymbol{\omega}) q = \frac{1}{2} \bar{S}(q)\boldsymbol{\omega}. \tag{A.7}$$

The linearization parts are given by

$$H_q = \frac{\partial(0.5 S(\boldsymbol{\omega})\mathbf{q}}{\partial \mathbf{q}}) = 0.5 S(\boldsymbol{\omega}) \tag{A.8}$$

$$H_w = \frac{\partial(0.5 S(\mathbf{q})\boldsymbol{\omega}}{\partial \boldsymbol{\omega}}) = 0.5 S(\mathbf{q}). \tag{A.9}$$

This gives the linearized states as

$$\dot{\mathbf{q}} = \begin{bmatrix} 0_{4\times 9} & S(\boldsymbol{\omega}) & S(\mathbf{q}) & 0_{4\times 8} \end{bmatrix} \mathbf{x} \tag{A.10}$$

Measurement linearization

There are three non linear measurement equation presented in Section 4.2.1, accelerometer, magnetometer and pitot tubes. The linear equations are not presented here and are unchanged from Section 4.2.1 when implementing the filter.

Accelerometer

The measurement equation, as in equation (4.19), is given by

$$\mathbf{y}^{\mathbf{acc}} = C_b^n(\mathbf{q})(\mathbf{a} - \mathbf{g}) - \mathbf{b}^{acc} + \mathbf{e}^{\mathbf{acc}}. \tag{A.11}$$

The rotation matrix $C_b^n(q)$ and acceleration $\mathbf{a} - \mathbf{g}$ is given by

$$C_b^n(\mathbf{q}) = \begin{bmatrix} q_0^2 + q_1^2 - q_2^2 - q_3^2 & 2(q_1 q_2 + q_0 q_3) & 2(q_1 q_3 - q_0 q_2) \\ 2(q_1 q_2 - q_0 q_3) & q_0^2 - q_1^2 + q_2^2 - q_3^2 & 2(q_2 q_3 + q_0 q_1 \\ 2(q_1 q_3 + q_0 q_2) & 2(q_2 q_3 - q_0 q_1) & q_0^2 - q_1^2 - q_2^2 + q_3^2 \end{bmatrix} \tag{A.12}$$

$$\mathbf{a} = \begin{bmatrix} a_N \\ a_E \\ a_D - g \end{bmatrix} \tag{A.13}$$

Taking the derivative with respect to $\mathbf{a}$, $\mathbf{q}$ and $\mathbf{b^{acc}}$ respectively gives

$$H_a^a = \left.\frac{\partial \mathbf{y_{acc}}}{\partial \mathbf{a}}\right|_{x=x_0} = C_b^n(\mathbf{q})|_{x=x_0} \tag{A.14}$$

$$H_q^a = \left.\frac{\partial \mathbf{y_{acc}}}{\partial \mathbf{q}}\right|_{x=x_0} = \begin{bmatrix} H_{q,1}^a \\ H_{q,2}^a \\ H_{q,3}^a \end{bmatrix} \tag{A.15}$$

$$H_a^b = I_{3\times 3} \tag{A.16}$$

where

$$H_{q,1}^a = \begin{bmatrix} \begin{bmatrix} q_0 \\ q_3 \\ -q_2 \end{bmatrix}^T \mathbf{a} & \begin{bmatrix} q_1 \\ q_2 \\ q_3 \end{bmatrix}^T \mathbf{a} & \begin{bmatrix} -q_2 \\ q_1 \\ -q_0 \end{bmatrix}^T \mathbf{a} & \begin{bmatrix} -q_3 \\ q_0 \\ q_1 \end{bmatrix}^T \mathbf{a} \end{bmatrix} \tag{A.17}$$

$$H_{q,2}^a = \begin{bmatrix} \begin{bmatrix} -q_3 \\ q_0 \\ q_1 \end{bmatrix}^T \mathbf{a} & \begin{bmatrix} q_2 \\ -q_1 \\ q_0 \end{bmatrix}^T \mathbf{a} & \begin{bmatrix} q_1 \\ q_2 \\ q_3 \end{bmatrix}^T \mathbf{a} & \begin{bmatrix} -q_0 \\ -q_3 \\ q_2 \end{bmatrix}^T \mathbf{a} \end{bmatrix} \tag{A.18}$$

$$H_{q,3}^a = \begin{bmatrix} \begin{bmatrix} q_2 \\ -q_1 \\ q_0 \end{bmatrix}^T \mathbf{a} & \begin{bmatrix} q_3 \\ -q_0 \\ -q_1 \end{bmatrix}^T \mathbf{a} & \begin{bmatrix} q_0 \\ q_3 \\ -q_2 \end{bmatrix}^T \mathbf{a} & \begin{bmatrix} q_1 \\ q_2 \\ q_3 \end{bmatrix}^T \mathbf{a} \end{bmatrix}. \tag{A.19}$$

The linearized measurement equation then becomes

$$y^{acc} = \begin{bmatrix} 0_{3\times 6} & H_a^a & H_q^a & 0_{3\times 3} & H_a^b & 0_{3\times 5} \end{bmatrix} \mathbf{x} \tag{A.20}$$

Magnetometer

The measurement equation, as in equation (4.28), is given by

$$\mathbf{y^{mag}} = C_b^n(q)\mathbf{B}^{earth} + \mathbf{e^{acc}} \tag{A.21}$$

The magnetic reference field generated by the earth is seen as a constant. The only non zero component in the measurement equation is then given by

$$H_q^m = \left.\frac{\partial \mathbf{y_{mag}}}{\partial \mathbf{q}}\right|_{x=x_0} = \begin{bmatrix} H_{q,1}^m \\ H_{q,2}^m \\ H_{q,3}^m \end{bmatrix} \tag{A.22}$$

where

$$H_{q,1}^m = \begin{bmatrix} \begin{bmatrix} q_0 \\ q_3 \\ -q_2 \end{bmatrix}^T \mathbf{B} & \begin{bmatrix} q_1 \\ q_2 \\ q_3 \end{bmatrix}^T \mathbf{B} & \begin{bmatrix} -q_2 \\ q_1 \\ -q_0 \end{bmatrix}^T \mathbf{B} & \begin{bmatrix} -q_3 \\ q_0 \\ q_1 \end{bmatrix}^T \mathbf{B} \end{bmatrix} \tag{A.23}$$

$$H_{q,1}^m = \begin{bmatrix} \begin{bmatrix} -q_3 \\ q_0 \\ q_1 \end{bmatrix}^T \mathbf{B} & \begin{bmatrix} q_2 \\ -q_1 \\ q_0 \end{bmatrix}^T \mathbf{B} & \begin{bmatrix} q_1 \\ q_2 \\ q_3 \end{bmatrix}^T \mathbf{B} & \begin{bmatrix} -q_0 \\ -q_3 \\ q_2 \end{bmatrix}^T \mathbf{B} \end{bmatrix} \tag{A.24}$$

$$H_{q,3}^m = \begin{bmatrix} \begin{bmatrix} q_2 \\ -q_1 \\ q_0 \end{bmatrix}^T \mathbf{B} & \begin{bmatrix} q_3 \\ -q_0 \\ -q_1 \end{bmatrix}^T \mathbf{B} & \begin{bmatrix} q_0 \\ q_3 \\ -q_2 \end{bmatrix}^T \mathbf{B} & \begin{bmatrix} q_1 \\ q_2 \\ q_3 \end{bmatrix}^T \mathbf{B} \end{bmatrix}. \tag{A.25}$$

The linearized magnetometer measurement then becomes

$$\mathbf{y}^{\mathbf{mag}} = \begin{bmatrix} 0_{3\times 9} & H_q^m & 0_{3\times 11} \end{bmatrix} \mathbf{x} \tag{A.26}$$